A literature review on sand transport under oscillatory flow conditions in the rippled-bed regime.

J.J. van der Werf

April 14, 2003

Abstract

The seabed is rarely flat. On the contrary, it tends to be covered with sedimentary structures with different time and spatial scales. The prevailing bedform type depends on the strength and the nature of the flow. Except for storm conditions, the largest part of the shoreface bed is covered with wave-induced ripples. Wave-induced ripples on the shoreface have typical heights of 0.01-0.1 m, lengths of 0.1-1.0 m, and migration speeds of 0.01-0.1 mms^{-1}.

Fundamentally different physical processes determine sand transport rates above plane and rippled sand beds. Above plane beds in oscillatory flow, momentum transfer occurs primarily by turbulent diffusion. In contrast, above rippled beds momentum transfer and the associated sediment dynamics in a near-bed layer with a thickness of about 1-2 ripple heights are dominated by coherent periodic vortex structures, whereas above this layer the coherent motions break down and are replaced by random turbulence. This leads to the entrainment of sand into suspension to considerably greater heights than above plane beds. In connection with sand transport, the phase of sand pick-up from the bottom during the wave-cycle is also significantly different above rippled beds with pick-up being linked to the phase of vortex shedding. This has potentially important consequences for the net sand transport rate beneath asymmetrical waves which can be negative (offshore) despite of larger positive (onshore) orbital velocities.

Experimental results are very important to understand the complex nature of sand transport. They give insight in the relevant processes and can be used to validate model concepts. Most of the laboratory experiments on wave-related transport processes are carried out in oscillating water tunnels and in wave flumes. There are large-scale and small-scale oscillating water tunnels and wave flumes. In large-scale tunnels and flumes, the velocities close to the bed and the wave periods can be comparable to the velocities occurring in nature. Therefore, it is possible to perform full-scale experiments. The simulated flow field in oscillating water tunnels differs from the flow field in nature (and from the flow field in wave flumes). In contrast with the orbital motion under real propagating waves, the same phase occurs at every location along oscillating water tunnels. Furthermore, vertical orbital motions are not simulated. A review of these laboratory data sets on wave-related transport mechanisms in the ripple regime shows the following.

1. During one wave cycle two concentration peaks occur above the ripple crest and ripple trough (lower peaks, larger time lags): one just after flow reversal probably generated by lee-side vortices and one around maximum flow probably generated by stoss-side vortices.

2. The phase of eddy shedding and suspended cloud ejection is possibly linked to the orbital diameter normalized with the ripple length.

3. The velocity and concentration fields above the ripple structure are so complex that it appears to be impossible to relate the local instantaneous sediment concentration to a local instantaneous fluid velocity.

4. There is empirical evidence that the vertical distribution of the time-averaged concentration (for symmetric, asymmetric, regular, and irregular waves) can be described with an analytical solution of the advection-diffusion equation with a constant decay length. However, proper expressions for this decay length and the reference concentration do not exist. The decay length is possibly linked to the ripple height.

5. Despite the larger onshore orbital velocities, the net wave-related transport over ripples is in most cases offshore-directed due to phase lags between velocities and concentrations caused by vortices on the lee-side of ripples.

6. The number of data sets on wave-related transport processes in the ripple regime with relatively large mobility numbers ($\Psi > 100$) and wave periods ($T > 5$ s) is limited. This especially accounts for time-dependent concentration and net transport measurements.

Since ripple geometry is a crucial parameter in the sand transport process, numerous studies have investigated the relation between wave parameters, grain size, and ripple geometry in laboratory and field settings usually adopting an empirical approach, e.g. Nielsen (1981), Vongvisessomjai (1984), Sato (1987), Mogridge *et al.* (1994), Wiberg & Harris (1994), and Sleath (2000). For typical field conditions large differences between the predicted ripple geometries occur. Moreover, the agreement between predicted ripple dimensions and experimental data is generally poor.

Many investigators have attempted to model the wave-related sand transport over ripples. These models can be divided into four groups: i)time-averaged models, ii)quasi-steady models, iii)semi-unsteady models, and iv)unsteady models. Time-averaged sand transport models, as often used in coastal engineering practice, are not capable to describe sand transport over ripples in wave-dominated conditions, because the wave-related transport component is not taken into account. Quasi-steady models are also not applicable in the ripple regime, because these models do not take phase differences between the instantaneous velocities and concentrations into account. Thus, only semi-unsteady and unsteady models are capable of predicting the wave-related sand transport rate in the ripple regime.

Semi-unsteady models take phase lags into account without describing the vertical distribution of the time-dependent horizontal velocity and sand concentration. In the literature two semi-unsteady models (among others) are described that try to parameterize the vortex process above ripples making use of experimental data sets: the grab-and-dump model of Nielsen (1988) and the model of Dibajnia & Watanabe (1992) adjusted by various researchers. The grab-and-dump model assumes that all sand entrained during onshore orbital motion is transported in offshore direction, and vice versa. Therefore, the predicted net wave-related transport is always negative (offshore-directed) under asymmetric waves, which is only realistic for a limited range of conditions. In the approach suggested by Dibajnia & Watanabe (1992) an expression is given for the total net transport rate, which is the difference between the amount of sand transported in positive (shoreward) and in negative (seaward) direction. Both consist of two parts: an amount of sand that is entrained and transported during the same half wave cycle and an amount of sand that is entrained during the preceding half wave cycle and transported during the next half wave cycle. The determinative parameter for the transport direction is the ratio of the fall time of sand particles to the bed and the half wave cycle period. If the fall time is longer than the wave crest (or trough) period, part of the entrained sand is transported in opposite direction. This process is modeled in a schematic way based on sheet-flow situations with adjustments to deal with rippled beds.

Unsteady models compute the unsteady flow velocity and sand concentration profiles with the appropriate boundary conditions. Afterwards the sand transport is averaged over the wave period in order to find the net sand transport. Unsteady models can be further divided into i)turbulence-closure models, ii)large eddy simulations, iii)direct numerical simulations, and iv)discrete-vortex models.

It is still not clear whether turbulence-closure models are able to represent coherent vortex dynamics realistically. Perrier (1996) compared the results of a discrete-vortex model and a Reynolds stress closure model and found that both models simulated the formation and shedding of vortices realistically. Perrier (1996) also found that higher-order Reynolds stress models should provide more accurate results than two-equation models. However, Andersen (1999) simulated the formation and shedding of vortices realistically with a two-equation k-ω closure model. The problem of applying LES and DNS on the seabed boundary layer is that rough sea beds are difficult to handle (Holmedal, 2002). DNS can only be applied on flows with moderate Reynolds number and simple geometries (Holmedal, 2002). Moreover, the calculations are very computational expensive. The major drawback against the discrete-vortex method is that it is essentially inviscid and therefore only a part of the

turbulent diffusion process can be simulated directly. Therefore sand can not be entrained to sufficient heights above the bed (Block *et al.*, 1994). It is important to notice that the real bottleneck in sand transport modeling over ripples is not the description of the hydrodynamics, but the sand transport description itself. Therefore, a sophisticated description of the hydrodynamics may be important, but it does not solve all uncertainties in computing the sand transport rate.

Most of the existing 1DV turbulence-closure models simply enhance their bed roughness to take the ripple effects into account. A comparison with experimental data showed that such models reproduce the time-averaged concentration and velocity profiles above ripples reasonably. However, the measured negative wave-related transport (thus against the direction of wave propagation) is generally not reproduced by the model (Sistermans, 2002). The model of Davies & Thorne (2002) is an attempt to parameterize the 2DV ripple effects in a 1DV model. For relatively flat ripples a "standard" 1DV flat bed model is applied with an increased bed roughness. For steeper ripples, the water column is divided into a lower vortex-dominated region and an upper turbulence-dominated region with a corresponding changeover level of two ripple heights above the (undisturbed) mean bed level. Ripple effects are accounted for by a strong time-varying but height-independent eddy viscosity, a larger sand diffusivity (mixing), and a strongly time-varying pick-up function as bottom boundary condition. A critical issue is the phase of vortex shedding and sand pick-up, which is considered to be independent of hydrodynamic and sedimentological conditions and modeled based on limited experimental and modeling evidence. More sophisticated are the 2DV turbulence-closure models where the ripple effects are modeled more directly (Andersen, 1999; Eidsvik, 2001; Silva, 2001).

Furthermore, it is concluded that:

1. Considering the present large uncertainties regarding the modeling of sediment dynamics in rippled-bed conditions, turbulence-closure models are appropriate *research* models to describe flow over ripples as a basis for sediment transport modeling.

2. Existing transport models, especially research models, are not well validated with experimental data in the ripple regime.

3. Intercomparison of both practical and research transport models shows that the greatest disagreement occurs in case of rippled beds.

4. 1DV modeling of sand transport by waves and currents in the ripple regime is a promising practical approach.

In the future the following research activities will be carried out: i)performance of new experimental series to obtain data sets of net transport rates, intra-wave transport processes, and other transport processes under both regular and irregular flow conditions in a range of full-scale field wave conditions as present on the shoreface, ii)improvement of existing semi-unsteady model concepts such as Nielsen (1988) and Dibajnia & Watanabe (1992) and development of new semi-unsteady models, iii)improvement of an existing 1DV turbulence-closure model following the ideas of Davies & Thorne (2002), and iv)assessment which of the two modeling concepts should be preferred for practical applications.

Contents

List of Figures

List of Tables

Chapter 1

Introduction

1.1 Background

Massive sand mining from the middle and lower shoreface (depths of 10 to 30 m) in large-scale pits will be required in many European countries in the near future. For example, around the North Sea and the Mediterranean Sea sand mining is necessary to nourish beaches and coastal dunes in response to increased coastal erosion due to the expected sea level rise. Furthermore, large-scale land reclamation and construction of large-scale artificial islands (for industrial purposes; ports and airports) in coastal seas -which are presently being considered- will also require huge amounts of sand as building material. Given the scale of these undertakings, the volume of sand required in the near future (10 to 20 years) will be of the order of 100 to 1000 million m^3 per country surrounding the North Sea (Sandpit project partners, 2001). To meet these demands, the existing sand mining areas need to be extended considerably and new potentially attractive areas should be explored and exploited.

The technical evaluation of the above-mentioned activities requires fundamental knowledge of morphological processes, sand transport processes, sand budgets, and ecology in the offshore coastal zones. The accurate determination of offshore and near-shore sand budgets is a primary problem in coastal zone management for many of the European coasts. Computed sand transport rates are highly uncertain, because of uncertainty associated with the validity of sand transport models in the shoreface environment. Comparisons between measured and predicted transport rates show differences up to two orders of magnitude (Davies *et al.*, 2002). Moreover, large uncertainty exists about whether sand is transported to the coast (onshore) or seaward (offshore) under the influence of waves (Silva, 2001; Sistermans, 2002). A main problem is the lack of model verification on data (particularly from the field).

On the shoreface four transport components can be distinguished: wave-related cross-shore transport, current-related cross-shore transport, wave-related longshore transport, and current-related longshore transport. My Ph.D. research and this literature review focusses on wave-related cross-shore transport, because i)wave-related transport mechanisms are still badly understood in comparison with current-related transport mechanisms and ii)cross-shore transport on the Dutch shoreface is dominated by the wave-related component due to wave asymmetry (Van der Werf, 2002). This wave asymmetry is present on the entire shoreface for moderate to extreme waves and in the shallower part for low to moderate waves. Finally, this research focusses on sand transport in the ripple regime, because i)except for storm conditions, the largest part of the shoreface bed is covered with wave-induced ripples (Van der Werf, 2002) and ii)in contrast to the sheet-flow (flat bed) regime, the transport mechanisms in the ripple regime are not well understood leading to a lack of reliable validated models for quantification of the transport processes in this regime.

1.2   Objective

The main objective of the Ph.D. project is: *to improve our understanding of wave-related sand transport mechanisms on the shoreface in the ripple regime under non-breaking waves and to develop reliable validated models for quantitative transport predictions on the basis of new and existing data (both field and laboratory) and existing transport model concepts.* The objective of this literature review is to gain insight in this research topic and in the state of the art.

1.3   Outline

This literature study consists of five chapters. After an introductory chapter, a description of the shoreface processes (particulary the ripple regime) is given in Chapter 2. Chapter 3 gives an overview of the laboratory experiments relevant for the research topic and in Chapter 4 existing sand transport models are described. In the concluding chapter the literature study is evaluated leading to conclusions and further research activities.

Chapter 2

Shoreface processes

2.1 Introduction

The shoreface is a morphological zone that lies between the surf zone and the inner continental shelf. This zone marks an important transition between the morphology and associated processes on the shelf and those of the surf zone and beach. Figure 2.1 shows the typical concave-upward profile of an open shoreface. Seabed slopes as steep as 1:50 are encountered near the surf zone, but these decrease
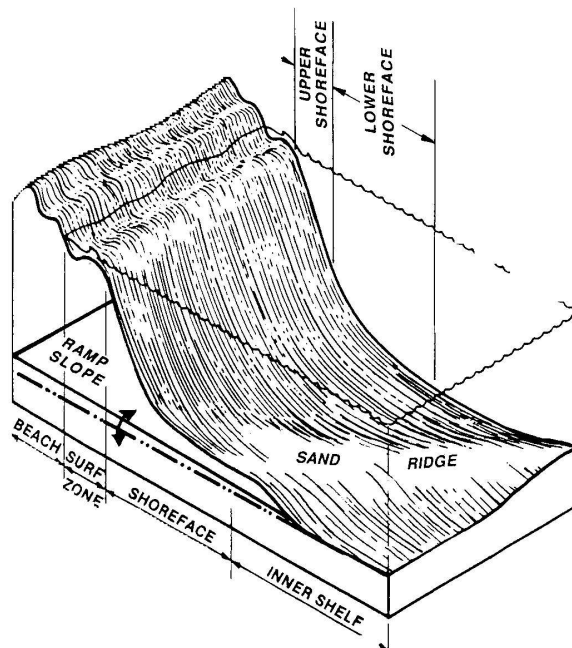
Figure 2.1: Diagram of the shoreface with the vertical dimension very exaggerated, after Niedoroda & Swift (1991).

to the order of 1:1,000 to 1:2,000 offshore where the shoreface merges with the gentle slope of the continental shelf (Everts, 1987). Data for the U.S. East and Gulf Coasts show that the shoreface width ranges between 2.1 and 25 km (average 8.7 km) and with outer depths ranging from 3.4 to 24.7 m (average 11.1 m) (Everts, 1978).

The shoreface is commonly divided into upper and lower regions. Niedoroda & Swift (1991) distinguish an inner or upper shoreface and an outer or lower shoreface. The upper shoreface generally lies between water depths of 4 and 11 m. The lower shoreface, which blends into the inner shelf,

generally begins at depths of 10 to 25 m. The flow on the upper shoreface is friction dominated. The lower shoreface is called the geostrophic zone with three dynamic "layers" being influenced by pressure gradients, friction, and the Coriolis force. Between the upper shoreface and the lower shoreface/inner shelf, there is a transition region where the friction-dominated zone blends into the three-layer geostrophic zone of the outer shoreface and adjoining shelf.

2.2   Hydrodynamics

2.2.1   Waves

The waves of greatest importance as far as the dynamics of the seabed are concerned are the *gravity waves* formed by wind action on the water surface. These wind waves have typical periods of 1-25 s and varying wave heights. These high-frequency waves are discussed in this section.

The range of water depths on the shoreface corresponds to depths where surface gravity waves undergo many important transitions. Waves are refracted and shoaled in these depths. They also change the shape of their surface profile, developing higher and more peaked crests and flatter and broader troughs. The corresponding wave orbital motions become characterized by larger and briefer onshore velocities followed by smaller and longer offshore velocities beneath wave troughs. This wave asymmetry is important for the sediment transport.

Water (indeed, any fluid) flowing near a solid surface is slowed down by friction along the boundary. The region of flow influenced by the proximity to the solid surface is called the boundary layer. In general the boundary layer thickness obeys the formula:

$$\delta \propto \sqrt{\nu_\text{t} T} \tag{2.1}$$

where ν_t is the eddy viscosity and T the flow period. The wave boundary layer δ_w remains normally very thin, generally a few millimeters over a smooth solid bed and a few centimeters over a flat bed of loose sediments. Bedforms, like ripples, may change the structure of the boundary layer by introducing strong rhythmic vortices. Hence, the wave boundary layer thickness over sharp-crested ripples can extend to four to five ripple heights or to a total of about 0.5 m under field conditions (Nielsen, 1992). Due to smaller velocities, boundary layer flow contains less inertia. Therefore, the flow can react more quickly to the varying pressure gradient. Consequently, the flow accelerates and decelerates more rapidly than the free stream and so the velocity inside the wave boundary layer is ahead in phase of the free stream velocity. For laminar flow over a smooth bed this phase lead is equal to $45°$. For rough turbulent flow the phase lead becomes smaller than $45°$.

For the case of an oscillating flow over a smooth plate the state of the flow is governed by the Reynolds number:

$$\text{Re}_\delta = \frac{\hat{u}\delta_\text{s}}{\nu} \tag{2.2}$$

with $\hat{u}$ the near-bed oscillating velocity amplitude, ν the kinematic viscosity, and δ_s the Stokes length defined as:

$$\delta_\text{s} = \sqrt{\frac{2\nu}{\omega}} \tag{2.3}$$

with $\omega = 2\pi/T$ the angular frequency. The flow is turbulent for $\text{Re}_\delta > 800$ and turbulent during the entire wave cycle for $\text{Re}_\delta > 3500$ (Jensen *et al.*, 1989). The flow is rough turbulent if the roughness Reynolds number $\text{Re}_* > 70$, transitional smooth-to-rough turbulent if $5 < \text{Re}_* < 70$, and smooth turbulent if $\text{Re}_* < 5$ (Schlichting, 1979). The roughness Reynolds number Re_* is defined as:

$$\text{Re}_* = \frac{u_* k_\text{s}}{\nu} \tag{2.4}$$

with $u_* = \sqrt{\tau_b/\rho}$ the friction velocity amplitude, τ_b the bed shear stress amplitude, ρ the density of water, and k_s the Nikuradse roughness height. For the case of a rough sea bottom the flow is often rough turbulent and thus independent of the Reynolds number in the sense that no viscous sublayer exists near the bottom.

The water under waves interacts with the seabed mainly through the bed shear stress $\tau_b(t)$. Hence, the determination of the bed shear stress is a crucial step in all sediment transport calculations. Jonsson (1966) defined the wave friction factor f_w in relation to the maximum bed shear stress $\tau_{b,max}$ by:

$$\tau_{b,max} = \frac{1}{2}\rho f_w \hat{u}^2 \tag{2.5}$$

The most well-known expression for the wave friction factor in the fully-developed rough turbulent regime is the formula of Swart (1974). The expression reads:

$$f_w = \exp\left[5.213\left(\frac{k_s}{a}\right)^{0.194} - 5.997\right] \tag{2.6}$$

with $a = \hat{u}\omega$ the semi-excursion length of orbital motion. Kajiura (1968) suggested $f_{w,max} = 0.25$ and Jonsson (1980) $f_{w,max} = 0.30$. However, measurements show values of f_w in excess of 0.5 or even in excess of 1.0 (Nielsen, 1992).

Under progressive waves water particles move along elliptic orbits, which are generally not completely closed. This can be explained by the fact that the horizontal velocity under the wave crest is slightly higher than under the wave trough. Therefore, the water particles will experience a net resulting displacement in the direction of the wave propagation. This phenomenon is called *Stokes drift*. The time-averaged Stokes drift velocity can be described by:

$$\bar{u}_s(z) = \frac{1}{8}\omega k H^2 \frac{\cosh 2kz}{\sinh^2 kh} \tag{2.7}$$

with $k = 2\pi/L$ the wave number, L the wave length, H the wave height, h the water depth, and z the vertical coordinate (positively upwards from the seabed). For waves propagating in a horizontally bounded domain the volume flux at each location usually equals zero. Therefore, the forward Stokes drift has to be compensated by a uniform return flow. This generates a positive velocity near the surface and a negative velocity near the bottom. The Stokes drift is of the order 0.01-0.1 ms^{-1}.

While the above-discussed velocity distributions might lead to the expectation of seaward net velocities near the bed, most measurements show actually a positive or shoreward net velocity close to the bed under non-breaking waves. This *boundary layer streaming* is caused by an additional mean shear stress generated by the fact that the horizontal and vertical velocities in a wave motion with a viscous bottom boundary layer are not exactly 90° out of phase as they would be in a perfectly inviscid wave motion. Boundary layer streaming has an order of magnitude similar to the Stokes drift velocity (Nielsen, 1992).

Under asymmetric waves additional offshore near-bed residual currents are generated due to turbulence asymmetry in successive wave half cycles, order 0.01-0.1 ms^{-1} (Ribberink & Al-Salem, 1994; Davies & Li, 1997).

In the surfzone another wave-generated current is present (and usually dominant): the so-called *undertow*. Undertow is a seaward mean velocity between the seabed and the wave trough level. It is a gravity-driven current related to the phenomenon of wave set-up.

2.2.2 Currents

Tide and wind are the dominant agents of shoreface currents. The response of the water mass is quite different in the inner and outer shoreface regions (see Section 2.1). These patterns can be further complicated by time lags and density stratification, see for more details Niedoroda & Swift (1991).

The wind-driven currents, both in cross-shore and long-shore direction, have typical velocities of 0.1-1.0 ms^{-1}. During storm events velocities up to 2.0 ms^{-1} have been measured (Niedoroda & Swift, 1991). Near-shore tidal currents tend to be oriented parallel to the isobaths. At the seaward limit of the shoreface these currents rotate in a flattened elliptical pattern. The dominantly coast-parallel orientation of shoreface tidal currents changes in areas with a standing component to the shelf tides. Typical velocities of tidal currents are 0.1-2.0 ms^{-1}. Strong and coherent currents develop in the shoreface as a results of the passage of long shelf waves with periods of the order of many hours to days. There are several types of long shelf waves depending on whether they consist primarily of deformations of the sea surface or deformations of the pycnocline (sharp density gradient). These non-locally forced currents (mainly longshore-oriented) have typical velocities of 0.01-0.1 ms^{-1}.

In contrast to the wave boundary layer, the current boundary layer is typically some metres or tens of metres thick. This indicates that on the shoreface the current boundary layer usually occupies the entire water column. The magnitude of the current-related bed shear stress depends mainly on the velocity profile. Assuming a logarithmic velocity profile, the expression for the time-averaged bed shear stress reads:

$$\bar{\tau}_{\rm c} = \frac{1}{2}\rho f_{\rm c}\bar{u}^2 \tag{2.8}$$

with $\bar{u}$ the time-averaged horizontal velocity at a near-bed level $z_{\rm u}$ outside the wave boundary layer and $f_{\rm c}$ the current friction factor defined by:

$$f_{\rm c} = 2\kappa \left[\ln\left(\frac{z_{\rm u}}{z_0}\right)\right]^{-2} \tag{2.9}$$

in which $\kappa = 0.4$ is the Von Karman constant and $z_0 = k_{\rm s}/30$ the level where the velocity is assumed to be zero.

2.2.3   Waves and currents

Both waves and currents play important roles in the sediment dynamics on the shoreface. The treatment in this case is complicated by the fact that waves and currents interact with each other hydrodynamically, so that their combined behaviour is not simply a linear sum of their separate behaviours. It is for example known that wave motion reduces the current velocities near the bed. The most important parameters for the wave-current interaction are the orbital velocity amplitude, the mean current velocity, and the angle between the wave and current. Waves and the currents interact mainly in two ways:

1. modification of the wave phase speed and wavelength by currents

2. interaction between the wave and current boundary layer

If the wave period is fixed, the wave length decreases if waves encounter an opposing current and consequently the wave height increases. The reverse happens with a following current. The component of a current perpendicular to the direction of the wave travel has no effect on the waves. Angles other than $\phi = 0°$, $\phi = 180°$, and $\phi = \pm 90°$ result in refraction of the wave by the current.

Nielsen (1992) concludes on the basis of absence of empirical evidence that the current-induced changes to the wave boundary layer structure can be ignored. Nielsen (1992) also provides information on the turbulence intensity in combined wave-current flows and the influence of waves on current velocity profiles.

The bed shear stress beneath combined waves and currents is enhanced beyond the value that would result from a simple linear addition of the wave-alone and the current-alone stress. This is caused by a non-linear interaction between the wave and current boundary layers. Several theories and models have been proposed to describe this process. Van Rijn (1993) and Soulsby (1997) give an overview of these theories and models. A possibility is to define a wave-current friction factor $f_{\rm cw}$

and determine the bed shear stress according to (2.5). Madsen & Grant (1976) give the following expression for this friction factor:

$$f_{\text{cw}} = \alpha f_{\text{c}} + (1 - \alpha) f_{\text{w}} \tag{2.10}$$

with

$$\alpha = \frac{\bar{u}}{\bar{u} + \hat{u}} \tag{2.11}$$

where the friction factors are determined using (2.6) and (2.9).

2.3 Bedforms

2.3.1 Introduction

The seabed is rarely flat. On the contrary, it tends to be covered with sedimentary structures with different time and spatial scales. The prevailing bedform type depends on the strength and the nature of the flow: steady current, tidal current, waves, or a combination of these. For water depths larger than about 20 m two types of large-scale seabed patterns can be distinguished: tidal sand banks and sand waves. In the more near-shore region shoreface-connected ridges, shoreface ridges, and longshore bars can be found. For a description see Blondeaux (2001). Furthermore, two types of small-scale bedforms are present on the shoreface with a different spatial and temporal scale:

- ripples with typical heights of 0.01-0.1 m, lengths of 0.1-1.0 m, and a temporal scale of seconds-minutes;

- megaripples with typical heights of 0.1-1.0 m, lengths of 1.0-10.0 m, and a temporal scale of hours-days.

Except for the spatial and temporal scale, these two ripple types differ with respect to their influence on the boundary layer structure and the sediment transport mechanisms. That is, over ripples, the suspended sediment distribution will scale on the ripple height, while for the megaripples the suspension distribution will scale on the flat bed boundary layer thickness which is much smaller than the height of those bedforms. This study focusses on the wave-induced ripples.

2.3.2 Coastal bedform regimes

Nielsen (1992) distinguishes three coastal bedform regimes based on the grain-roughness Shields parameter. This grain-roughness Shields parameter is defined by:

$$\theta_{2.5} = \frac{\frac{1}{2} f_{2.5} \hat{u}^2}{\Delta g D_{50}} \tag{2.12}$$

with $f_{2.5}$ the friction factor based on (2.6) with a roughness of $2.5 D_{50}$, D_{50} the grain size for which 50% of the sediment (by weight) is smaller, $\Delta = (\rho_{\text{s}} - \rho)/\rho$ the relative density of sediment, and ρ_{s} the density of sediment. If the flow is too weak to cause appreciable sediment motion ($\theta_{2.5} < 0.05$), the bed topography will be dominated by relict bedforms or the seabed is plane. Under flows of intermediate strength ($0.05 \leq \theta_{2.5} < 1.0$) the bed will be covered with bedforms which are more or less in equilibrium with the flow conditions. Focussing on wave-action, wave-induced ripples will be present in this Shields regime. Under very vigorous flows ($\theta_{2.5} \geq 1.0$) bedforms cannot exist and the bed is usually flat. However, megaripples have been found under such conditions.

2.3.3 Wave-induced ripples

The ripples first appearing on a flat bed subject to wave-action have been called *rolling-grain ripples* by Bagnold (1946). In this stage close to inception of motion, the grains that are entrained from the bed start to roll back and forth on top of the flat bed. After a while they collect together and form small triangular ridges: rolling-grain ripples. According to Bagnold (1946), these ripples are stable if the Shields parameter is less than two times the critical value. For more vigorous flows, the lee-side vortex becomes so strong that it is able to initiate grain motion in the space between the two ripples. In this case the ripples grow until the equilibrium geometry of these so-called *vortex ripples* is reached. Stable rolling-grain ripples are rarely found in the field and during laboratory experiments. It seems as if rolling-grain ripples are always developing into vortex ripples, but the transition period can be very long if the grain motion is close to threshold (Andersen, 1999).

Clifton (1976) introduced a different classification of wave-induced ripples based on the ratio of the orbital diameter $d_{\mathrm{o}} = 2a$ and the grain size. Clifton (1976) distinguishes the following three types:

- orbital ripples for $d_{\mathrm{o}}/D_{50} < 1000$, the length increases with increasing d_{o} and is independent of D_{50};

- suborbital ripples for $1000 < d_{\mathrm{o}}/D_{50} < 5000$, the length decreases with increasing d_{o} and increases with increasing D_{50};

- anorbital ripples for $d_{\mathrm{o}}/D_{50} > 5000$, the length is independent of d_{o} and increases with increasing D_{50}.

Observations of wave-induced ripples show that orbital ripples are characterized by a constant steepness of roughly 0.17 (Wiberg & Harris, 1994). Anorbital ripples have a maximum steepness smaller than this, closer to 0.12, and the steepness decreases with increasing orbital diameter until sheet-flow conditions are reached. Suborbital ripples have an intermediate steepness. Wiberg & Harris (1994) show that most of the orbital ripples were observed in flumes, whereas most of the anorbital ripples were observed in the field. Both flume and field data comprise suborbital ripples. For field conditions, ripples have been found with lengths up to 0.9 m and with heights up to 0.15 m (Van Rijn, 1993). The ripple geometry can be either 2D or 3D depending on the energy conditions. Sato (1987) estimates the maximum asymmetry of ripples:

$$\left(\frac{\lambda_{\mathrm{c}}}{\lambda}\right)_{\max} = 0.61 \tag{2.13}$$

with λ_{c} the length of an offshore facing flank of a ripple. This relation appears to explain the trend of the experimental data in strongly asymmetric flows (Sato, 1987).

When co-directional currents are superimposed on waves, wave-induced ripples tend to migrate in the current direction and become asymmetric with steeper downstream faces. In case of perpendicular or near-perpendicular currents two ripple systems may co-exist according to the relative current strength. For an overview of different ripples under action of combined waves and currents see Amos *et al.* (1988).

Blondeaux *et al.* (2000) found by accounting for a steady drift beneath steep waves that rolling-grain ripples migrate at a constant rate which is predicted as a function of sediment and wave characteristics. Faraci & Foti (2001) present experimental evidence that the trend in the migration rate of vortex ripples is the same as that given by the theoretical findings of Blondeaux *et al.* (2000). Faraci & Foti (2001) also found that the velocity of ripple migration in presence of irregular waves is almost the same as for regular waves characterized by the same wave energy. The order of magnitude of ripple migration is 0.01-0.1 $\mathrm{mm\,s}^{-1}$.

2.3.4 Ripple predictors

The most widely-used ripple predictors are developed by Nielsen (1981) and Wiberg & Harris (1994). Nielsen (1981) developed two sets of empirical relationships for ripple length, ripple height, and

ripple steepness on the basis of extensive laboratory data and some field data. One for laboratory data (regular waves) and the other for field data (irregular waves). For laboratory conditions the expressions read:

$$\frac{\lambda}{a} = 2.2 - 0.345\Psi^{0.34} \qquad (2 < \Psi < 232) \tag{2.14}$$

$$\frac{\eta}{a} = 0.275 - 0.022\Psi^{0.5} \qquad (\Psi < 156) \tag{2.15}$$

$$\frac{\eta}{\lambda} = 0.182 - 0.24\theta_{2.5}^{1.5} \qquad (\theta_{2.5} < 0.83) \tag{2.16}$$

and for field conditions:

$$\frac{\lambda}{a} = \exp\left(\frac{693 - 0.37\ln^8\Psi}{1000 + 0.75\ln^7\Psi}\right) \tag{2.17}$$

$$\frac{\eta}{a} = 21\Psi^{-1.85} \qquad (\Psi > 10) \tag{2.18}$$

$$\frac{\eta}{\lambda} = 0.342 - 0.34\sqrt[4]{\theta_{2.5}} \tag{2.19}$$

in which λ the ripple length, η the ripple height, and the mobility number Ψ defined by:

$$\Psi = \frac{\hat{u}^2}{\Delta g D_{50}} = \frac{2\theta_{2.5}}{f_{2.5}} \tag{2.20}$$

which does not take the bed roughness into account. The advantage of the ripple predictor of Nielsen (1981) is that it is relatively simple. Disadvantages are: i)the distinction between field and laboratory conditions and ii)the difference between the predicted ripple steepness and the ratio of the predicted ripple height and length.

Wiberg & Harris (1994) developed for each ripple type (orbital, suborbital, and anorbital) empirical relationships to predict ripple length, ripple height, and ripple steepness. There is substantial overlap with the data set used by Nielsen (1981). At first, the anorbital ripple length and height are determined with:

$$\lambda_{a} = 535D_{50} \tag{2.21}$$

$$\frac{\eta_{a}}{\lambda_{a}} = \exp\left[-0.095\left(\ln\frac{d_{o}}{\eta_{a}}\right)^2 + 0.442\ln\frac{d_{o}}{\eta_{a}} - 2.28\right] \tag{2.22}$$

Then the ripple type is determined: orbital ripples for $d_{o}/\eta_{a} < 20$, suborbital ripples for $20 < d_{o}/\eta_{a} < 100$, and anorbital ripples for $d_{o}/\eta_{a} > 100$. For orbital ripples the expressions read:

$$\lambda_{o} = 0.62d_{o} \tag{2.23}$$

$$\frac{\eta_{o}}{\lambda_{o}} = 0.17 \tag{2.24}$$

and in case of suborbital ripples:

$$\lambda_{s} = \exp\left[\left(\frac{\ln(d_{o}/\eta_{a}) - \ln 100}{\ln 20 - \ln 100}\right)(\ln\lambda_{o} - \ln\lambda_{a}) + \ln\lambda_{a}\right] \tag{2.25}$$

with the suborbital ripple height and steepness computed using (2.22) and (2.25). The single framework for both field and laboratory conditions is an advantage of the ripple predictor of Wiberg & Harris. The main disadvantage is the determination of the ripple type in advance.

Other prediction methods for wave-induced are developed by Vongvisessomjai (1984), Sato (1987), and Mogridge *et al.* (1994), all based on an extensive set of laboratory and field data. Vongvisessom-jai (1984) distinguishes growing or vortex ripples and decaying or turbulent ripples. Vongvisessomjai (1984) uses a *ripple function* as discriminator: growing ripples for $\Psi_\mathrm{R} = \sqrt{\Psi} \cdot a/D_{50} < 5500$, decaying ripples for $\Psi_\mathrm{R} > 5500$, and an "optimum ripple" for $\Psi_\mathrm{R} = 5500$. Vongvisessomjai (1984) concludes that growing ripples are two-dimensional and decaying ripples three-dimensional. Design curves depending on the period parameter $\chi = D_{50}/\left(\Delta g T^2\right)$ were developed to compute the ripple geometry. Sato (1987) concludes that the ripple dimensions differ strongly for 2D- and 3D-ripples. For regular, irregular, symmetric, and asymmetric flows the range of 2D-ripples can be described with $d_\mathrm{o}/D_{50} < 1500$ and $\theta_{2.5} < 0.9 \left(d_\mathrm{o}/D_{50}\right)^{-0.25}$. For both ripple types (with a distinction between regular and irregular flows), Sato (1987) relates the ripple dimensions to the coupled parameter $d_\mathrm{o}/D_{50} \cdot \sqrt{\theta_{2.5}}$. Mogridge *et al.* (1994) also conclude that there is a strong dependence of the ripple length and height on the period parameter χ. Mogridge *et al.* (1994) present a prediction method where the maximum ripple length and height (and accompanying orbital diameter) depend on the period parameter. Using these parameters, the actual ripple length and height can be determined. This prediction procedure is largely based on the work of Mogridge & Kamphuis (1972).

O'Donoghue & Clubb (2001) compared measured ripple dimensions and ripple dimensions predicted by the methods of Nielsen (1981), Vongvisessomjai (1984), Wiberg & Harris (1994), and Mogridge *et al.* (1994). O'Donoghue & Clubb (2001) conclude that for relatively small values of the period number χ -corresponding to typical field conditions- large differences between the predicted ripple geometries occur. From their experimental work O'Donoghue & Clubb (2001) conclude that the Wiberg & Harris (1994) and Vongvisessomjai (1984) method are unreliable for field-scale conditions and recommend the method of Mogridge *et al.* (1994) for ripple predictions.

2.3.5 Influence ripples

Wave-induced ripples have no immediate impact on the main flow patterns, but they strongly influence the boundary layer structure and the turbulence intensity near the bed. Hence, they have great influence on the sediment transport. The most straightforward way to take the ripple influence into account is to summarize the ripple geometry in terms of the Nikuradse roughness height k_s. In absence of ripples (or any bedform) only skin friction is present and the roughness height is related to the grain diameter, e.g. $k_\mathrm{s} = 2.5 D_{50}$. If ripples are present they generate form drag. This results in an increase in the total friction exerted on the bed and a roughness height of the order of the ripple height. A simple rule to account for the ripple influence on the bed roughness is:

$$k_\mathrm{s} = r \frac{\eta^2}{\lambda} \tag{2.26}$$

with r a constant. Constant r is of the order 10, e.g. Nielsen (1992) suggested $r = 8$ and Van Rijn (1993) $r = 20$. This approach is only valid for cases where the horizontal scale of orbital motion is much larger than the horizontal scale of the bedforms: $d_\mathrm{o} \gg \lambda$.

Several methods have been developed to relate the bed roughness and the ripple geometry, e.g. Grant & Madsen (1982) and Raudkivi (1990). Usually a component related to the sediment transport is added to the total friction. In the ripple and sheet-flow regime the grain-related roughness is negligible small compared to the components related to the bedforms and sediment transport.

2.4 Sediment transport

2.4.1 Introduction

Sediment starts to move if the mobilizing forces are larger than the stabilizing forces. The mobilizing forces acting on sediment grains are lift and drag forces caused by fluid moving over the sediment.

The gravity force forms the stabilizing force. The ratio of these forces determines the ability to move the grain. This ratio is called Shields parameter:

$$\theta_{2.5}(t) = \frac{\frac{1}{2}f_{2.5}u^2(t)}{\Delta g D_{50}} \tag{2.27}$$

This Shields parameter only includes skin friction, because the form drag does not affect the stability of individual sediment grains. If this Shields parameter exceeds a critical value (threshold of motion or inception of motion) sediment is transported. For a more detailed description of inception of motion see e.g. Nielsen (1992) and Van Rijn (1993).

2.4.2 Transport modes

Three different transport modes are distinguished:

- wash load;

- bedload;

- suspended load.

Bagnold (1956) defines bedload as that part of the total load that is supported by intergranular forces. Suspended load and wash load are supported by fluid drag. Wash load consists of very fine particles which are transported by the water and which are normally not represented in the bed. Therefore, the knowledge of bed composition does not permit any prediction of the rate of wash load transport. Hence, wash load is neglected computing the total sediment discharge on the basis of the local seabed characteristics. Bedload can also be described as the part of the total load that is in almost continuous contact with the bed carried forward by rolling, sliding, or hopping. Suspended load is the part of the total sediment transport that is maintained in suspension by turbulence in the flowing water for considerable periods of time without contact with the bed. It moves with practically the same (horizontal) velocity as that of flowing water.

2.4.3 Transport regimes

Classically, sediment transport under waves is divided into three distinct regimes:

- bedload regime;

- ripple regime;

- sheet-flow regime.

There is no sediment motion for very small values of the Shields parameter. The critical Shields parameter depends on the sediment size, sediment density, fluid viscosity, and flow structure. For natural conditions the critical Shields parameter varies between 0.03 and 0.06. If the Shields parameter exceeds the critical value, sediment particles start to roll, slide, and jump over each other, but the bed remains flat (or covered with relict bedforms). Intergranular forces are important because the particles are in almost continuous contact with the bed and with each other. The sediment is transported as bedload in a layer of a few grain sizes thick. If the Shields parameter increases further, bedforms are developed. An indication of the value of the Shields parameter at this transition from the bedload regime to the ripple regime is unknown. It is likely that under dominant oscillatory flow this transition occurs rapidly after inception of motion. The transport mode over these bedforms is either bedload or suspended load depending on the ratio of the friction velocity to the particle fall velocity u_*/W_{f}. For even larger values of the Shields parameter ($\approx$ 0.8-1.0) ripples are washed out and the bed becomes plane. A thin layer with high sediment concentrations (100-1000 kgm^{-3}) is moving in a sheet along the bed. The thickness of this sheet-flow layer is about 10-100 grain sizes.

2.4.4   Transport components

Sediment transport has a current-related and a wave-related component. Current-related transport is the transport component as a result of the product of the time-averaged components of the flow and sediment concentration and wave-related transport is the transport component as a result of the product of the time-varying components of flow and sediment concentration during the wave cycle.

To demonstrate the difference between these two transport components, the instantaneous velocity and concentration can be decomposed in two components:

$$u(t) = \bar{u} + \tilde{u}(t) \tag{2.28a}$$
$$c(t) = \bar{c} + \tilde{c}(t) \tag{2.28b}$$

with $\bar{u}$ the time-averaged cross-shore velocity, $\tilde{u}$ the oscillating velocity component in cross-shore direction, $\bar{c}$ the time-averaged concentration, and $\tilde{c}$ the oscillating concentration component. The net cross-shore transport at a particular vertical level can be obtained by averaging over the wave period:

$$\langle q_{\mathrm{s}} \rangle = \frac{1}{T} \int_0^T uc \, \mathrm{d}t = \overline{uc} \tag{2.29}$$

Substitution of (2.28) in (2.29) yields:

$$\overline{uc} = \bar{u}\bar{c} + \overline{\tilde{u}\tilde{c}} \tag{2.30}$$

with $\bar{u}\bar{c}$ the current-related flux and $\overline{\tilde{u}\tilde{c}}$ the wave-related flux.

Consider a situation where short wind waves propagate in x-direction and a tidal current is present with velocity u_0 under an angle α, see Figure 2.2. Using the basic transport formula $q_{\mathrm{s}} = m|u|^2 u$
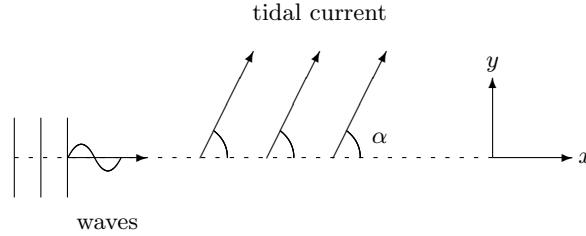
Figure 2.2: Situation sketch.

(with m a proportionality constant), the wave- and current-related transport components can be determined. The orbital motion is modeled with a second-order Stokes theory, taking the asymmetry of the waves into account:

$$\tilde{u}(t) = \hat{u}_1 \cos(\omega t) + \hat{u}_2 \cos(2\omega t) \tag{2.31}$$

with $\hat{u}_1$ and $\hat{u}_2$ the orbital velocity amplitudes of the first and second harmonic component. The velocity vector:

$$\vec{u}_{\mathrm{r}}(t) = (\tilde{u}(t) + u_0 \cos\alpha, u_0 \sin\alpha) \tag{2.32}$$
$$|\vec{u}_{\mathrm{r}}(t)|^2 = \tilde{u}^2(t) + u_0^2 + 2u_0\tilde{u}(t)\cos\alpha \tag{2.33}$$

leads to the following current-related transport:

$$\langle \vec{q}_{\mathrm{s,c}}(t) \rangle = \left\langle m|\vec{u}_{\mathrm{r}}(t)|^2 \vec{u}_0 \right\rangle \tag{2.34}$$

$$= m \left(u_0^3 + \frac{1}{2}u_0\hat{u}_1^2 + \frac{1}{2}u_0\hat{u}_2^2 \right) \tag{2.35}$$

and the following wave-related transport:

$$\langle \vec{q}_{s,w}(t) \rangle = \left\langle m |\vec{u}_r(t)|^2 \vec{\tilde{u}}(t) \right\rangle \tag{2.36}$$

$$= m \left(\frac{3}{4} \hat{u}_1^2 \hat{u}_2 + u_0 \hat{u}_1^2 \cos\alpha + u_0 \hat{u}_2^2 \cos\alpha \right) \tag{2.37}$$

The first term on the right-hand side of (2.35) and (2.37) indicate current- and wave-related transport respectively, while the other terms are extra transport components due to the wave-current interaction.

2.4.5 Sediment transport in the ripple regime

Fundamentally different physical processes determine sediment transport rates above plane and rippled sediment beds. Above plane beds in oscillatory flow, momentum transfer occurs primarily by turbulent diffusion. In contrast, above rippled beds momentum transfer and the associated sediment dynamics in the near-bed layer are dominated by coherent motions, specifically by the process of vortex formation above ripple lee slopes and the shedding of these vortices around flow reversal. Above steep long-crested ripples, this well-organized vortex process is highly effective in entraining sediment into suspension. In a near-bed layer with a thickness of 1-2 times the ripple height, the flow dynamics are dominated by these coherent periodic vortex structures, whereas above this layer the coherent motions break down and are replaced by random turbulence (Davies & Villaret, 1997). This leads to the entrainment of sediment into suspension to considerably greater heights than above plane beds. In connection with sediment transport, the phase of sediment pick-up from the bottom during the wave-cycle is also significantly different above rippled beds with pick-up being linked to the phase of vortex shedding. This has potentially important consequences for the net sediment transport rate beneath asymmetrical waves which can be negative (offshore) despite of larger positive (onshore) orbital velocities. The underlying mechanism of this wave-related transport against the wave propagation in case of asymmetrical waves is the existence of phase differences between the peak concentrations and peak velocities related to the generation of vortices on the lee-side of steep ripples. In general, phase lags are more important for finer sediment and shorter periods. This typical process for transport over steep ripples and the transport process in case of plane beds is illustrated in Figure 2.3.

Davies & Villaret (1997) present an overview of experimental studies on oscillatory flow above rippled beds and conclude that a good detailed description of the near-bed oscillatory flow above ripples has been achieved. In a near-bed layer with a thickness of 1-2 times the ripple height, the flow dynamics are dominated by coherent periodic vortex structures which are generated above the ripple lee slope in each wave half-cycle and then ejected above the crest just after flow reversal. However, Block *et al.* (1994) present experimental evidence that the moment of ejection can happen just before or just after flow reversal depending on d_o/λ. The intensity of each vortex and its lifetime depend on the wave Reynolds number (Re) as well as on the details of the ripple shape (sharp- or round-crested), steepness, and skin roughness. The lifetime of coherent vortices is approximately one wave cycle after which they break down into isotropic small-scale turbulence.

2.5 Dimensional analysis

It is useful to know which parameters determine the flow and sand transport over ripples and hence the geometry of ripples. These dimensional parameters are combined to non-dimensional quantities using a dimensional analysis. Table 2.1 shows the dimensional parameters involved in the combined asymmetric oscillatory and steady flow and sediment transport over ripples. With 13 dimensional parameters and three primary dimensions (mass, time and space), it is possible to form 10 non-dimensional quantities. The orbital diameter d_o sets the most important length scale. Table 2.2 shows these non-dimensional quantities.
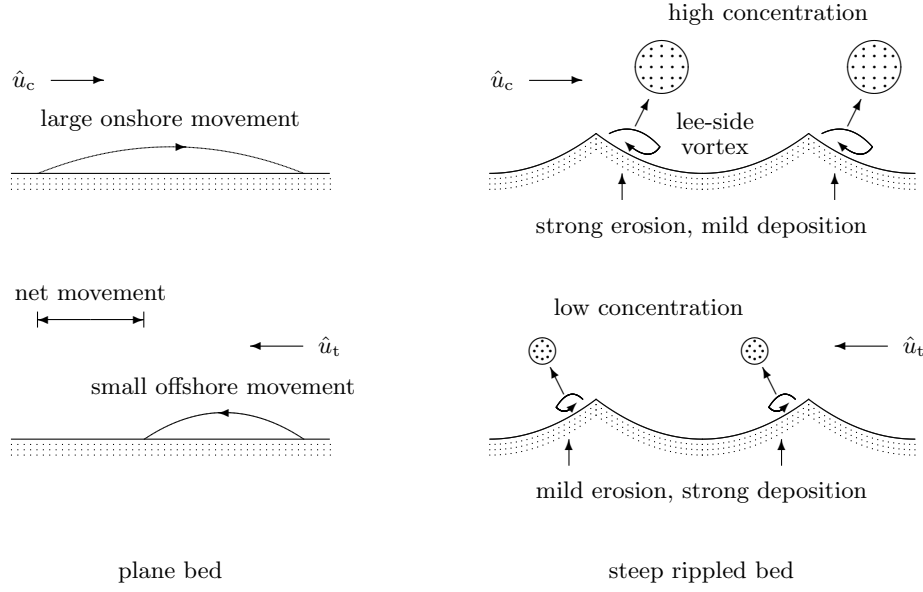
Figure 2.3: Transport processes in asymmetric wave motion over a plane and steep rippled bed, after Van Rijn (1993).

Parameter	Symbol	Primary dimensions
acceleration due to gravity	g	$[\mathrm{LT^{-2}}]$
density of water	ρ	$[\mathrm{ML^{-3}}]$
kinematic viscosity of water	ν	$[\mathrm{L^2T}]$
wave period	T	$[\mathrm{T}]$
maximal orbital velocity	$\hat{u}_\mathrm{c}$	$[\mathrm{LT^{-1}}]$
minimal orbital velocity	$\hat{u}_\mathrm{t}$	$[\mathrm{LT^{-1}}]$
current strength	$\bar{u}$	$[\mathrm{LT^{-1}}]$
density of sediment	ρ_s	$[\mathrm{ML^{-3}}]$
median grain size	D_{50}	$[\mathrm{L}]$
particle fall velocity	W_f	$[\mathrm{LT^{-1}}]$
ripple height	η	$[\mathrm{L}]$
ripple length	λ	$[\mathrm{L}]$
sand transport	q_s	$[\mathrm{L^2T^{-1}}]$

Table 2.1: Dimensional parameters determining the flow and sand transport over ripples.

Parameter	Description/process
d_o/D_{50}	relative orbital diameter
$\mathrm{Re}_{d_o} = (\hat{u}_\mathrm{c} d_\mathrm{o})/\nu$	characterization flow
$\hat{u}_\mathrm{c}/\hat{u}_\mathrm{t}$	wave asymmetry
$\hat{u}_\mathrm{c}/\bar{u}$	wave/current strength ratio
u_*/W_f	suspension parameter
Δ	relative density of sediment
η/λ	ripple steepness
d_o/λ	relative ripple length
$\theta_{2.5}$	sediment mobility
$\Phi = q_\mathrm{s}/(D_{50}W_\mathrm{f})$	sand transport

Table 2.2: Non-dimensional quantities determining the flow and sand transport over ripples.

Chapter 3

Experiments

3.1 Introduction

Experimental results are very important to understand the complex nature of sand transport. They give insight in the relevant processes and can be used to validate model concepts. Most of the laboratory experiments on wave-related transport processes are carried out in oscillating water tunnels and in wave flumes. There are large-scale and small-scale oscillating water tunnels and wave flumes. In large-scale tunnels and flumes, the velocities close to the bed and the wave periods can be comparable to the velocities occurring in nature. Therefore, it is possible to perform full-scale experiments. The simulated flow field in oscillating water tunnels differs from the flow field in nature (and from the flow field in wave flumes). In contrast with the orbital motion under real propagating waves, the same phase occurs at every location along oscillating water tunnels. Furthermore, vertical orbital motions are not simulated.

Field experiments are scarce, because they are difficult to perform, expensive, and the validity of the results is often questionable. This applies especially for field measurements in the shoreface environment with relatively large water depths. In this section laboratory experiments in the ripple regime are described, focussing on wave-related transport processes. For a review of field experiments reference is made to Kleinhans (2002) and for laboratory experiments in the sheet-flow regime to Janssen (1995) and Van Rijn *et al.* (2001). For older experimental work in the laboratory the interested reader is referred to a literature review by Ribberink (1989).

3.2 Instantaneous concentrations

Bosman (1981, 1982) was one of the first to measure instantaneous sediment concentrations generated by regular waves over rippled beds in a small-scale oscillating water tunnel. Typical conditions were: $D_{50} = 0.14\text{-}0.21$ mm, $T = 1\text{-}3$ s, and $\hat{u} = 0.27\text{-}0.35$ ms^{-1}. Figure 3.1 show ensemble mean values of instantaneous concentrations within a wave cycle measured by Bosman (1982). A sinusoidal oscillatory motion with a period $T = 1$ s and a velocity amplitude of $\hat{u} = 0.3$ was generated over a uniform sand bed ($D_{50} = 0.20$ mm). The bed was covered with almost perfect 2D ripples ($\eta = 0.01$ m, $\lambda = 0.055$ m). The following phenomena can be observed above the ripple crest:

- relatively large (random) scatter (roughly ±50%);

- two large concentration peaks just after flow reversal, probably generated by lee-side vortices;

- two smaller concentration peaks at the moment of maximum flow, probably generated by stoss-side vortices.

The phenomena above the ripple trough were (not shown here):
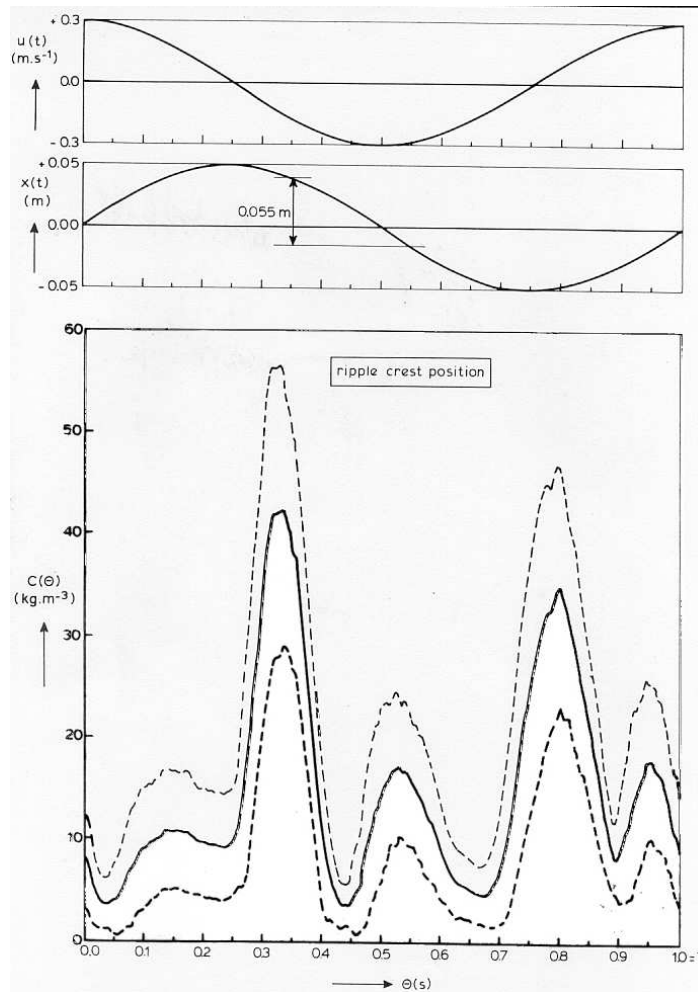
Figure 3.1: Ensemble mean values and standard deviations of instantaneous concentrations over a wave cycle 10 mm above the ripple crest, after Bosman (1982).

- relatively large (random) scatter;

- two large concentration peaks just after flow reversal, probably generated by lee-side vortices (time lag is larger compared to concentration measurements above the crest);

- two smaller concentration peaks after maximum flow, probably generated by stoss-side vortices;

- smaller peaks above the ripple trough than above the ripple crest due to diffusion and settling of sediment particles.

Strangely enough the concentration distribution is asymmetric, while the water motion is symmetric.

Block et $al.$ (1994) measured instantaneous sediment concentrations under regular sinusoidal waves in a small-scale wave flume with $D_{50} = 0.09$ mm, $T = 2$ s, and $\hat{u} = 0.16$ and 0.26 ms^{-1}. Results show that the moment of suspended cloud ejection can be just before or just after flow reversal depending on d_o/λ.

Instantaneous concentrations were also measured by Chen (1992) (small-scale wave flume), Dang Huu & Grasmeijer (1999) (large-scale wave flume), Grasmeijer & Van Rijn (1999) (small-scale wave flume), Clubb (2001) (large-scale oscillating water tunnel), Grasmeijer (2002) (large-scale wave flume), Sistermans (2002) (small-scale wave flume), and Thorne et $al.$ (2002) (large-scale wave flume). All

laboratory experiments show that the velocity and concentration fields above the ripple structure are so complex that it appears to be impossible to relate the local instantaneous sediment concentration to a local instantaneous fluid velocity.

3.3 Time-averaged concentrations

Time-averaged concentrations are relevant for the current-related or *advective* sediment transport. In case of oscillatory flow over a rippled bed, the instantaneous sediment concentrations vary both in time and space. To eliminate these variations, it is necessary to average the concentrations over time (many waves) and space (many bedforms). This can be achieved by slowly moving the measurement instrument horizontally back and forth the test section. Time-averaged sediment concentrations in the ripple regime have been measured by:

- Chen (1992), Block *et al.* (1994), Grasmeijer & Van Rijn (1999), and Sistermans (2002) in a small-scale wave flume;

- Dang Huu & Grasmeijer (1999), Grasmeijer (2002), and Thorne *et al.* (2002) in a large-scale wave flume;

- Bosman (1981, 1982) and Ribberink (1987) in a small-scale oscillating water tunnel (concentrations are also bed-averaged);

- Ribberink & Al-Salem (1989, 1991b, 1992), Ramadan (1994), Ribberink (1995), and Clubb (2001) in a large-scale oscillating water tunnel.

The vertical distribution of time- and bed-averaged sediment concentration is often described with an advection-diffusion model in which the vertically downward sediment flux induced by gravity is compensated by an upward flux induced by the vertical mixing process:

$$w_{\mathrm{s}} c + \varepsilon_{\mathrm{s}} \frac{\partial c}{\partial z} = 0 \tag{3.1}$$

with w_{s} the settling velocity of the sediment in suspension and ε_{s} the sediment mixing coefficient. Based on an extensive data set of measurements in the ripple regime and using (3.1), Bosman & Steetzel (1988) show that the vertical distribution of time- and bed-averaged sediment concentration can be described with a constant ε_{s}:

$$\bar{c}(z) = c_0 \exp\left(-\frac{z w_{\mathrm{s}}}{\varepsilon_{\mathrm{s}}}\right) \tag{3.2}$$

where z is the vertical coordinate with respect to the average bed level (spatially averaged over the ripples). Bosman & Steetzel (1988) give the following expression for the (extrapolated) concentration at $z = 0$ (in kgm^{-3}):

$$c_0 = G \frac{\hat{u}^{3.5}}{T^2} \tag{3.3}$$

with G a proportionality factor, $G = 3000 \pm 8$ kgm$^{6.5}$s$^{5.5}$. For the concentration decay length r_{c} ($= \varepsilon_{\mathrm{s}}/W_{\mathrm{f}}$) the following relation was obtained by Steetzel (1984):

$$r_{\mathrm{c}} = R_0 \frac{T}{W_{\mathrm{f}}} \tag{3.4}$$

with R_0 a proportionality factor, $R_0 = 2.2 \cdot 10^{-4}$ m^{2}s^{-2}. Especially the bed concentration c_0 was well described by (3.3) over almost four orders of magnitude ($\pm 20\%$). The relation of r_{c} is only valid for relatively large orbital velocities (with an accuracy of $\pm 10\%$ for $\hat{u} \geq 0.35$ ms^{-1}).

On the basis of measured $\bar{c}(z)$-profiles and the simple exponential profile (3.2), Nielsen (1986) suggested the formula:

$$c_0 = 0.005\theta_{\rm r}^3 \tag{3.5}$$

This formula for c_0 applies reasonably well for both rippled and flat beds, see Nielsen (1986). The modified effective Shields parameter $\theta_{\rm r}$ is given by:

$$\theta_{\rm r} = \frac{\theta_{2.5}}{(1 - \pi\eta/\lambda)^2} \tag{3.6}$$

with the grain-roughness Shields parameter calculated with (2.27). The correction factor $(1 - \pi\eta/\lambda)^2$ is the square of the velocity correction suggested by Du Toit & Sleath (1981) for the flow enhancement near the crest of vortex ripples (Nielsen, 1992).

Ribberink (1987) studied the influence of wave asymmetry and wave irregularity on the time- and bed-averaged sediment concentration profiles above ripples. Ribberink (1987) performed two series of experiments (A to study wave asymmetry, B to study wave irregularity) using a grain size of 0.21 mm. Table 3.1 shows the experimental conditions. Ribberink (1987) concludes that the time-

Series	Wave type	$T_{\rm (p)}$ (s)	$\tilde{u}$ (ms^{-1})	η (m)	λ (m)
A	asymmetric	3.0-5.0	$\hat{u}_1 = 0.35,$	0.023-0.035	0.165-0.260
			$\hat{u}_2 = 0.00, 0.07$		
B	irregular,	1.9-5.9	$\hat{u}_{\rm s} = 0.20\text{-}0.51$	0.010-0.018	0.055-0.135
	asymmetric				

Table 3.1: Experimental conditions and ripple characteristics (Ribberink, 1987).

and bed-averaged sediment concentration profile in case of asymmetric and irregular waves can fully described by (3.2). Ribberink (1987) further concludes that:

- an additional harmonic causes an average increase of $\approx 25\%$ in the reference concentration c_0;

- the concentration decay length $r_{\rm c}$ decreases due to wave asymmetry ($\approx 10\%$) and wave irregularity ($\approx 25\text{-}50\%$);

- wave asymmetry does not influence the ripple dimensions, but wave irregularity lowers all ripple dimensions.

Ribberink (1987) suggests the following expressions for the reference concentration:

$$\text{asymmetric waves} \quad c_0 = G\left(\frac{\hat{u}_{\rm c}^{3.5}}{4TT_{\rm c}} + \frac{\hat{u}_{\rm t}^{3.5}}{4TT_{\rm t}}\right) \tag{3.7}$$

$$\text{irregular waves} \quad c_0 = G\frac{\hat{u}_{\rm eff}^{3.5}}{T_{\rm p}^2} \tag{3.8}$$

with G the proportionality factor of Bosman & Steetzel (1988), $\hat{u}_{\rm c}$ the maximum velocity under the wave crest, $\hat{u}_{\rm t}$ the maximum velocity under the wave trough, $T_{\rm c}$ the crest period, $T_{\rm t}$ the trough period, $T_{\rm p}$ the peak period of the wave spectrum, and $\hat{u}_{\rm eff} = 1.62\sqrt{m_0}$ the effective velocity amplitude with m_0 the variance of the velocity signal.

Ribberink & Al-Salem (1994) analyzed the data sets of Ribberink & Al-Salem (1989, 1991b, 1992) who measured time-averaged concentrations for three series of experiments with a grain size of 0.21 mm. The experimental conditions are shown in Table 3.2. Based on this data set and data of Ribberink (1987) and Bosman & Steetzel (1988), Ribberink & Al-Salem (1994) conclude that the concentration decay length is strongly correlated to the ripple height. In the velocity range $0.2 \leq \hat{u}_{\rm rms} \leq 0.42$ ms^{-1} and for a wide range of ripple heights (factor 100) a good fit (within a factor

Series	Wave type	$T_{(p)}$ (s)	$\hat{u}_{rms}$ (ms^{-1})	η (m)	λ (m)
A1	sinusoidal	2.0-10.0	0.21-0.42	0.016-0.090	0.137-0.763
A2	sinusoidal	2.0-10.0	0.64-1.06	0.125-0.350	0.830-2.700
B	irregular, asymmetric	5.0-9.1	0.20-0.32	0.003-0.014	0.084-0.110

Table 3.2: Experimental conditions and ripple characteristics (Ribberink & Al-Salem, 1994).

2) is obtained with the simple linear relation $r_c \approx \eta$. This strong correlation was already noticed by Ribberink (1987). Ribberink & Al-Salem (1994) physically explain this correlation for fully-developed ripples by the fact that the diameter of (coherent) vortices determines the length scale of the sediment mixing process in the near-bed layer above the ripples. Visual observations showed that the dimensions of the vortices are approximately the same as the ripple heights. Ribberink & Al-Salem (1994) conclude that the empirical relation for the bed concentration (3.3) appears to be also valid in full-scale conditions with fully-developed ripples during series A1 and B.

The strong relation between the vertical scale of sand concentration r_c and the ripple height η over sharp-crested was also noticed by Nielsen (1990) who suggested:

$$r_c = \begin{cases} 0.075 \frac{a\omega}{w_s}\eta & \text{for } \frac{a\omega}{w_s} < 18 \\ 1.4\eta & \text{for } \frac{a\omega}{w_s} > 18 \end{cases} \tag{3.9}$$

It has been argued, particularly by Nielsen (1992) on the basis of field data of Nielsen (1984) and laboratory data of McFetridge & Nielsen (1985), that both convective and diffusive mechanisms are involved in the entrainment process and that a combined description of these processes is therefore necessary. In this approach the steady state advection-diffusion equation is given by:

$$w_s c + \varepsilon_s \frac{\partial c}{\partial z} - w_s c_0 F(z) = 0 \tag{3.10}$$

with $F(z)$ a function describing the probability of a particle reaching height z above the bed. The respective terms in (3.10) represent downward settling, upward diffusion, and upward convection. The form of the convective entrainment function proposed by Nielsen (1992) is:

$$F(z) = (1 + z/l)^{-\xi} \tag{3.11}$$

with l an appropriate vertical length scale. For power ξ Nielsen (1992) suggested a value of 2 on the basis of the data of McFetridge & Nielsen (1985).

More recently, Sistermans (2002) measured time-averaged suspended sediment concentrations under irregular asymmetric waves (JONSWAP spectrum) and a co-linear current in a (small-scale) wave flume. Sistermans (2002) performed two test series with graded sediment ($D_{90}/D_{10} = 5$) and one with uniform sediment ($D_{90}/D_{10} = 2$). Experimental conditions for the uniform case were: $D_{50} = 0.17$ mm, $H_s = 0.12\text{-}0.19$ m, $T_p = 2.5$ s, $\bar{u} = 0.00\text{-}0.36$ ms^{-1} (following), $\eta = 0.6\text{-}2.5$ cm, and $\lambda = 8.8\text{-}21.9$ cm. These experiments show that the near-bed reference concentration c_b does not depend on the grading of the bed material. Furthermore, higher suspended sediment concentrations were found for graded sediment over the entire vertical except close to the bed.

Thorne *et al.* (2002) measured time-averaged concentration profiles in a large-scale wave flume under both regular and irregular weakly asymmetric waves over rippled beds with $D_{50} = 0.33$ mm, $T = 4\text{-}6$ s, and $\Psi = 12\text{-}82$. Thorne *et al.* (2002) conclude that the empirical expression of Nielsen (1986) for the reference concentration c_o (3.5) shows reasonably overall agreement with the measurements in respect of the dependence of c_o on the Shields parameter; but the formula somewhat overestimates the measured concentrations. Furthermore, Thorne *et al.* (2002) conclude that in a near-bed layer of thickness about two times the ripple heights, pure diffusion characterized by a height-independent sediment diffusivity with the decay length scale of Nielsen (1990) (3.9) provides a good representation of the measured profiles. Above this, Nielsen (1992) convection-diffusion solution (3.10) provides a better representation.

3.4   Sediment transport rates

Sediment transport rates under short (high-frequency) waves have been investigated by many researchers. However, most of these were performed in the sheet-flow regime. There are two principle ways to measure the (net) transport rate. The first is by using the sediment balance method: at both sides of the test section sediment traps are place and the collected sediment is weighted. Another method is to measure the instantaneous velocity and concentration at different heights above the bed. The total (suspended) transport rate through the measuring cross-section is then computed by integration of the mean value of the product of these two:

$$\langle q_{\mathrm{s}} \rangle = \int\limits_{z_{\mathrm{b}}}^{h} \langle uc \rangle \ \mathrm{d}z \qquad (3.12)$$

where z_{b} is a near-bed reference level.

Sato (1987) performed experiments in a small-scale oscillating water tunnel with sediment of 0.18 mm in the ripple regime. Both regular and irregular asymmetric oscillatory flows were generated. In nearly all tests the net transport rate was in backward direction, while the largest peak velocity was in the forward direction.

Chen (1992) measured both the instantaneous velocity and concentration in a small-scale wave flume. Figure 3.2 shows both the total sediment flux ($\overline{uc}$) and that due to mean flow ($\bar{u} \cdot \bar{c}$). Conditions were: sinusoidal wave with opposing current of 0.08 ms^{-1}, $T = 1.76$ s, $\hat{u} = 0.189$ ms^{-1}, $D_{50} = 0.18$ mm, $\eta = 2$ cm, and $\lambda = 8$ cm. This figure shows that the flux due to oscillatory flow is small
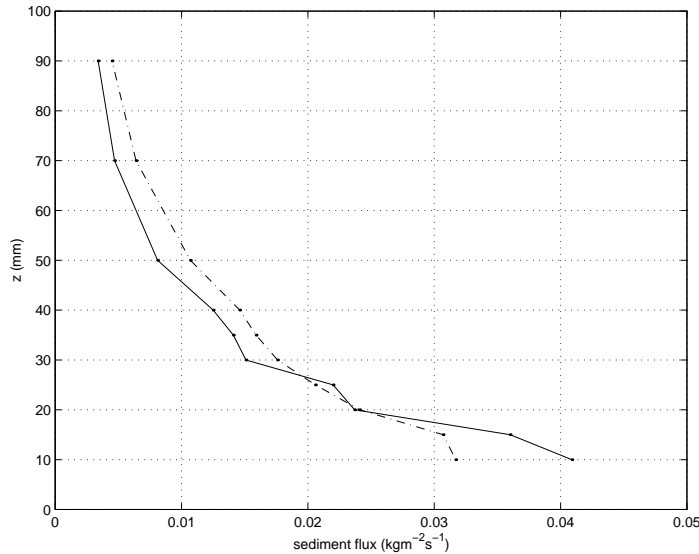
Figure 3.2: Vertical distribution of sediment fluxes above the ripple crest. The solid line represents the total flux ($\overline{uc}$) and the dashed line the flux due to mean flow ($\bar{u} \cdot \bar{c}$). The fluxes are in absolute values, which are all against the wave direction because of the mean current and a return flow compensating for the mass transfer in the wave direction (Chen, 1992).

compared to the flux due to mean flow. Near the ripple crest the wave-related transport is in the same direction as the current-related transport. In the upper zone, the direction of the wave-related transport is opposite from the direction of the current-related transport.

Net transport under waves in the ripple regime has also been measured by Ribberink & Al-Salem (1989, 1991b, 1992), Watanabe & Isobe (1990) (small-scale oscillating water tunnel), Hassan *et al.* (1999) (large-scale oscillating water tunnel), Clubb (2001), and Grasmeijer (2002).

3.5 Overview experiments

In Table 3.3 an overview of experiments with non-breaking waves over a rippled uniform sandbed is presented. These are carried out in small-scale wave flumes (swf), large-scale wave flumes (lwf), small-scale oscillating water tunnels (sowt), and large-scale oscillating water tunnels (lowt). This

reference	fac. type	flow type	D_{50} (mm)	T (s)	Ψ (-)	measured parameters				
						η	λ	$c(z)$	$c(z,t)$	q_s
Bosman (1981, 1982)	sowt	rs	0.22	1.0-5.0	10-101	x	x	x	x	
Ribberink (1987)	sowt	rs	0.21	3.0-5.0	36	x	x	x		
		ra	0.21	3.0-5.0	38	x	x	x		
		ia	0.21	1.9-5.9	11-77	x	x	x		
Sato (1987)	sowt	rs	0.18	0.5-7.0	7-145	x	x			
		ra	0.18	3.0-5.0	12-87	x	x			x
		is	0.18	4.0-5.2	4-24	x	x			
		ia	0.18	3.7-5.2	6-96	x	x			x
Watanabe & Isobe (1990)	sowt	ra	0.18,0.87	3.0-6.0	6-66					x
Chen (1992)	swf	ra	0.20	1.8	7	x	x	x	x	x
Ribberink & Chen (1993)	lowt	ia	0.13	6.5,9.1	28-139	x	x			
Block *et al.* (1994)	swf	rs	0.09	2	18,46	x	x	x	x	
Ramadan (1994)	lowt	rs	0.21	7.0	47-424	x	x			
		ra	0.21	6.5	53	x	x	x		
Ribberink & Al-Salem (1994)	lowt	rs	0.21	2.0-10.0	27-662	x	x	x		
		ia	0.21	5.0-9.1	24-64	x	x	x		x
Ribberink (1995)	lowt	ra	0.21	6.5	53,147	x	x			
Dang Huu & Grasmeijer (1999)	lwf	ia	0.16,0.33	5	40-130	x	x	x	x	
Grasmeijer & Van Rijn (1999)	swf	ia	0.10	2.3	37-54	x	x	x	x	
Hassan *et al.* (1999)	lowt	ra	0.97	6.5	46-103	x	x			x
Clubb (2001)	lowt	rs	0.16-0.44	2.0-10.0	15-125	x	x			
		rs,ra	0.34	5.0,10.0	52,87	x	x	x	x	
		ra	0.34	5.0,10.0	52-104	x	x			x
Grasmeijer (2002)	lwf	ia	0.23	6.0	143	x	x	x	x	x
Sistermans (2002)	swf	ia	0.17	2.5	19-50	x	x	x	x	
Thorne *et al.* (2002)	lwf	ra	0.33	4.0-6.0	22-82	x	x	x	x	
		ia	0.33	4.9-5.1	12-70	x	x	x	x	

Table 3.3: Overview of data sets on wave-related transport processes under non-breaking waves over a rippled uniform sandbed obtained in small-scale wave flumes (swf), large-scale wave flumes (lwf), small-scale oscillating water tunnels (sowt), and large-scale oscillating water tunnels (lowt) with different flow types: regular symmetric oscillations (rs), regular asymmetric oscillations (ra), irregular symmetric oscillations (is), and irregular asymmetric oscillations (ia).

table shows that the number of data sets on time-averaged concentrations and ripple dimensions is fairly large. However, the number of time-dependent and net transport measurements in large-scale experimental facilities is limited. This especially accounts for high mobility numbers ($\Psi > 100$) and long periods ($T > 5$ s).

Chapter 4

Sediment transport models

4.1 Introduction

In this chapter an overview of the existing mathematical models that describe and quantify the sediment transport processes in the ripple regime is presented. For an overview of transport models in the flat bed (sheet-flow) regime see Janssen (1995) and Van Rijn *et al.* (2001). For older models the interested reader is referred to a literature review by Ribberink (1989).

Sediment transport models can be divided into four groups:

- time-averaged models;

- quasi-steady models;

- semi-unsteady models;

- unsteady models.

These four model types will be discussed in the next sections.

4.2 Time-averaged models

Time-averaged models were the first models that were developed to derive the sediment transport rate under waves and currents. The sediment transport rate is described at a time scale much longer than the wave period using the wave-averaged values of velocity and concentration:

$$\bar{q}_{\mathrm{s}} = \int_0^h \bar{u}(z) \cdot \bar{c}(z) \, \mathrm{d}z \tag{4.1}$$

with $\bar{u}(z)$ and $\bar{c}(z)$ the time-averaged velocity and concentration respectively. A widely-used time-averaged transport formula is developed by Bijker (1971). This formula describes the current-related transport (suspended load and bedload) with waves acting as stirring agent. The influence of ripples can be taken into account by adding an extra shear stress related to the bedforms. The total net transport is always in the direction of the mean current. The disadvantage of this approach is that the wave-related transport component is not taken into account. Therefore, time-averaged models are not further considered in this literature review.

4.3   Quasi-steady models

Quasi-steady models are based on the assumption that the instantaneous transport rate is directly related to a certain power of the instantaneous near-bed flow velocity or bed shear stress. In this approach the wave-related transport as well as the wave-current interaction are implicitly accounted for. The behaviour of quasi-steady models can be illustrated by considering a situation of an asymmetric (second-order Stokes) wave superimposed on a net current:

$$u(t) = \bar{u} + \hat{u}_1 \cos(\omega t) + \hat{u}_2 \cos(2\omega t) \tag{4.2}$$

The net transport rate can be described with:

$$\bar{q}_s = m \frac{1}{T} \int_0^T u^3(t) \, \mathrm{d}t \tag{4.3}$$

Substitution of (4.2) in (4.3) and integration over the wave period leads to the following expression for the net transport:

$$\bar{q}_s = m \left(\bar{u}^3 + \frac{3}{2} \bar{u} \hat{u}_1^2 + \frac{3}{2} \bar{u} \hat{u}_2^2 + \frac{3}{4} \hat{u}_1^2 \hat{u}_2 \right) \tag{4.4}$$

The first three terms on the right-hand side of (4.4) are current-related transport components with extra components induced by stirring of both the first and second harmonic waves. The last term represents the wave-related transport component due to wave asymmetry.

One of the most widely-used quasi-steady models is the Bailard (1981) formula. It is a total load formula for both waves and currents and bed slopes in any direction. The effect of ripples can be represented using a ripple-related roughness.

The response of sediment transport to velocity changes can be considered instantaneous if the phase lag between the sediment concentration (or sediment transport) and the velocity is small compared to the time scale on which the velocity varies, i.e. wave period T. Dohmen-Janssen (1999) concludes that in sheet-flow conditions phase lags are significant when the following criterion is fulfilled:

$$P = \frac{\delta_{sf} \omega}{W_f} = 2\pi \frac{t_{fall}}{T} > 0.5 \tag{4.5}$$

with P the phase lag parameter and δ_{sf} the sheet-flow layer thickness. Experimental evidence (Ribberink & Al-Salem, 1994) shows that for a large range of conditions the suspension decay height over rippled beds scales with the ripple height. Analogous to sheet-flow conditions, the expression for the phase lag parameter reads:

$$P = 2\pi \frac{\eta}{W_f T} > 0.5 \tag{4.6}$$

If $W_f = 2.6 \cdot 10^{-2}$ ms^{-1} ($D_{50} \approx 0.2$ mm), $T = 7$ s, and $\eta = 0.04$ m the phase lag parameter $P = 1.4$, which indicates the significance of phase lags. Quasi-steady models are therefore not valid in the ripple regime, because of the existence of phase differences between the instantaneous velocities and concentrations due to eddy motions at the lee-side of the ripples. This latter phenomena is especially important in case of steep vortex ripples.

4.4   Semi-unsteady models

Semi-unsteady models take phase lags into account without describing the vertical distribution of the time-dependent horizontal velocity and sand concentration.

4.4.1 Watanabe (1982)

Watanabe (1982) proposed the following empirical relation for the dimensionless wave-related net transport rate:

$$|\Phi| = \frac{\langle q_\mathrm{s} \rangle}{W_\mathrm{f} D_{50}} = 7\left(\theta'_\mathrm{on} - \theta'_\mathrm{cr}\right)\sqrt{\theta'_\mathrm{on}} \tag{4.7}$$

with:

$$\theta'_\mathrm{on} = \frac{1}{2} f'_\mathrm{w} \frac{\hat{u}_\mathrm{c}^2}{\Delta g D_{50}} \tag{4.8}$$

and where θ'_cr (= 0.11) represents the critical Shields parameter corresponding to the threshold for the general movement of sediment particles. This formula only predicts the magnitude of the net transport and does not give the transport direction.

Sato (1987) compared this formula with a large data set of net sand transport rates in the ripple regime under regular and irregular asymmetric waves obtained in a small-scale oscillatory water tunnel with $D_{50} = 0.18$ mm, $T = 3.0\text{-}5.2$ s, and $\Psi = 4\text{-}96$. Sato (1987) shows that this formula gives reasonably good predictions of the *absolute* sediment transport under both regular and irregular asymmetric flow above ripples except for irregular flow with low values of the Shields parameter.

4.4.2 Nielsen (1988)

Nielsen (1988) developed a simple grab-and-dump model to describe the wave-related sediment transport over ripples. The basic idea is that sediment is entrained ("grabbed") in two parcels each wave period by the escaping lee-side vortices at the times of free stream reversal. The amounts entrained after forward and backward velocities respectively are $A_\mathrm{f} c_{0,\mathrm{s}} W_\mathrm{f} T$ and $A_\mathrm{b} c_{0,\mathrm{s}} W_\mathrm{f} T$ with $c_{0,\mathrm{s}}$ the reference concentration for a sine wave with velocity amplitude $\hat{u}_1$ computed using (3.5). A_f and A_b are entrainment coefficients to account for wave asymmetry:

$$A_\mathrm{f} = 0.5 \left(\frac{\hat{u}_\mathrm{max}}{\hat{u}_1}\right)^6 \tag{4.9}$$

$$A_\mathrm{b} = 0.5 \left(\frac{\hat{u}_\mathrm{min}}{\hat{u}_1}\right)^6 \tag{4.10}$$

with $\hat{u}_\mathrm{max}$ and $\hat{u}_\mathrm{min}$ the shoreward and seaward extreme velocities respectively and $\hat{u}_1$ the orbital velocity amplitude of the first harmonic. In each case the sediment is then transported the average distance a in the direction opposite to the velocities that entrained the sediment and then deposited ("dumped"). This leads to the following amount of sand carried by $u(\mathrm{t})$ during one wave period:

$$V = c_{0,\mathrm{s}} W_\mathrm{f} T \left(A_\mathrm{b} - A_\mathrm{f}\right) a \tag{4.11}$$

and the corresponding time-averaged wave-related sediment transport:

$$\langle q_\mathrm{s} \rangle = c_{0,\mathrm{s}} W_\mathrm{f} \left(A_\mathrm{b} - A_\mathrm{f}\right) a \tag{4.12}$$

Nielsen (1988) validated this model with wave flume data from Schepers (1978) and Tilmans (1979) who measured the sediment transport in the ripple regime under second-order Stokes waves and a small co-linear current in a small-scale wave flume. Experimental conditions were $D_{50} = 0.087\text{-}0.465$ mm, $T = 1.5$ and 1.7 s, and $\Psi = 6\text{-}30$.

4.4.3 Dibajnia & Watanabe (1992)

Dibajnia & Watanabe (1992) present an expression for the total net transport rate, which is the difference between the amount of sediment transported in positive (shoreward) and in negative (seaward) direction. Both consist of two parts: an amount of sediment that is entrained and transport during the same half wave cycle and an amount of sediment that is entrained during the preceding half wave cycle and transported during the next half wave cycle. This behaviour is expressed by the non-dimensional parameter Γ:

$$\Gamma = \frac{u_{\mathrm{c}} T_{\mathrm{c}} \left(\Omega_{\mathrm{c}}^3 + \Omega_{\mathrm{t}}'^3\right) - u_{\mathrm{t}} T_{\mathrm{t}} \left(\Omega_{\mathrm{t}}^3 + \Omega_{\mathrm{c}}'^3\right)}{(u_{\mathrm{c}} + u_{\mathrm{t}}) \, T} \tag{4.13}$$

with T_{c} and T_{t} the time during which the velocity is positive and negative respectively. u_{c} and u_{t} represent the equivalent sinusoidal velocity amplitudes of the positive and the negative wave cycle:

$$u_{\mathrm{c}}^2 = \frac{2}{T_{\mathrm{c}}} \int_0^{T_{\mathrm{c}}} u^2 \, \mathrm{d}t \tag{4.14}$$

$$u_{\mathrm{t}}^2 = \frac{2}{T_{\mathrm{t}}} \int_{T_{\mathrm{c}}}^{T} u^2 \, \mathrm{d}t \tag{4.15}$$

Values of Ω_{c}, Ω_{c}', Ω_{t}, and Ω_{t}' are obtained as follows:

$$\text{if } \omega_{\mathrm{c}} \leq \omega_{\mathrm{cr}} \begin{cases} \Omega_{\mathrm{c}} & = \omega_c \frac{2 W_{\mathrm{f}} T_{\mathrm{c}}}{D_{50}} \\ \Omega_{\mathrm{c}}' & = 0 \end{cases} \tag{4.16}$$

$$\text{if } \omega_{\mathrm{c}} > \omega_{\mathrm{cr}} \begin{cases} \Omega_{\mathrm{c}} & = \omega_{\mathrm{cr}} \frac{2 W_{\mathrm{f}} T_{\mathrm{c}}}{D_{50}} \\ \Omega_{\mathrm{c}}' & = (\omega_{\mathrm{c}} - \omega_{\mathrm{cr}}) \frac{2 W_{\mathrm{f}} T_{\mathrm{c}}}{D_{50}} \end{cases} \tag{4.17}$$

$$\text{if } \omega_{\mathrm{t}} \leq \omega_{\mathrm{cr}} \begin{cases} \Omega_{\mathrm{t}} & = \omega_t \frac{2 W_{\mathrm{f}} T_{\mathrm{t}}}{D_{50}} \\ \Omega_{\mathrm{t}}' & = 0 \end{cases} \tag{4.18}$$

$$\text{if } \omega_{\mathrm{t}} > \omega_{\mathrm{cr}} \begin{cases} \Omega_{\mathrm{t}} & = \omega_{\mathrm{cr}} \frac{2 W_{\mathrm{f}} T_{\mathrm{t}}}{D_{50}} \\ \Omega_{\mathrm{t}}' & = (\omega_{\mathrm{t}} - \omega_{\mathrm{cr}}) \frac{2 W_{\mathrm{f}} T_{\mathrm{t}}}{D_{50}} \end{cases} \tag{4.19}$$

with:

$$\omega_{\mathrm{c}} = \frac{T_{\mathrm{fall}}}{T_{\mathrm{c}}} = \frac{u_{\mathrm{c}}^2}{2 \Delta g W_{\mathrm{f}} T_{\mathrm{c}}} \tag{4.20}$$

$$\omega_{\mathrm{t}} = \frac{T_{\mathrm{fall}}}{T_{\mathrm{t}}} = \frac{u_{\mathrm{t}}^2}{2 \Delta g W_{\mathrm{f}} T_{\mathrm{t}}} \tag{4.21}$$

The non-dimensional net transport rate Φ_{s} is then:

$$|\Phi_{\mathrm{s}}| = \frac{q_{\mathrm{s}}}{W_{\mathrm{f}} D_{50}} = 0.001 \, |\Gamma|^{0.55} \frac{\Gamma}{|\Gamma|} \tag{4.22}$$

The original Dibajnia & Watanabe model was developed for sheet-flow conditions with a critical value ω_{cr} of 1. Dibajnia & Watanabe (1992) remark that the model concepts generally hold, though in a different scale, for sediment transport over ripples. Dibajnia & Watanabe (1992) suggest to change the critical value from unity to a value of 0.001 to take account of the fact that usually most of the sediment suspended during one half cycle is carried by the velocity of the coming successive half

cycle. This model is validated with data of Sunamura (1982), Sato (1987), and Watanabe & Isobe (1990). Watanabe & Isobe (1990) measured the net transport rate in a small-scale oscillatory water tunnel over a rippled bed under second-order Stokes waves with $D_{50} = 0.18$ and 0.87 mm, $T = 3$ and 6 s, and $\Psi = 6\text{-}86$. However, there is ambiguity about this critical value. After an experimental study on sediment transport, Suzuki *et al.* (1994) propose a value of 0.03 for rippled-bed conditions. Dibajnia *et al.* (1994) propose a generalization of the Dibajnia & Watanabe (1992) formula for the case of rippled beds with ω_{cr} a function of the Shields parameter:

$$\omega_{cr} = 1 - 0.97\sqrt{1 - \left[(\theta_{2.5} - 0.2)/0.4\right]^2} \cdot \min(1, 2\lambda/d_o) \tag{4.23}$$

The last term takes care of the fact that when the orbital diameter is much larger than the ripple length, the net transport should be in onshore direction.

4.4.4 Dibajnia & Watanabe (1996)

The transport formula of Dibajnia & Watanabe (1992) is based on experimental data using (uniform) sediment with a median grain size of 0.2 mm. Dibajnia & Watanabe (1996) generalized this model for different grain sizes and different densities using data of Sawamoto & Yamashita (1986) who measured half-cycle averaged transport rates in the sheet-flow regime under sinusoidal oscillations and new data on transport rates under cnoidal waves over plane and rippled beds with a sand mixture of fine ($D_{50} = 0.20$ mm) and coarse ($D_{50} = 0.87$ mm) sand. The general expression for the sediment transport reads:

$$|\Phi_s| = \frac{q_s}{W_f D_{50}} = 0.0015\,|\Gamma|^{0.5}\,\frac{\Gamma}{|\Gamma|} \tag{4.24}$$

ω_c, ω_t, Γ, u_c, and u_t are computed using the equations derived by Dibajnia & Watanabe (1992). The differences between the original and the new model of Dibajnia & Watanabe are the expressions for Ω_j:

$$\text{if } \omega_c \le \omega_{cr} \begin{cases} \Omega_c &= \omega_c T_c \sqrt{\frac{\Delta g}{D_{50}}} \\ \Omega' &= 0 \end{cases} \tag{4.25}$$

$$\text{if } \omega_c > \omega_{cr} \begin{cases} \Omega_c &= \omega_{cr} T_c \sqrt{\frac{\Delta g}{D_{50}}} \\ \Omega'_c &= (\omega_c - \omega_{cr}) T_c \sqrt{\frac{\Delta g}{D_{50}}} \end{cases} \tag{4.26}$$

$$\text{if } \omega_t \le \omega_{cr} \begin{cases} \Omega_t &= \omega_t T_t \sqrt{\frac{\Delta g}{D_{50}}} \\ \Omega'_t &= 0 \end{cases} \tag{4.27}$$

$$\text{if } \omega_t > \omega_{cr} \begin{cases} \Omega_t &= \omega_{cr} T_t \sqrt{\frac{\Delta g}{D_{50}}} \\ \Omega'_t &= (\omega_t - \omega_{cr}) T_t \sqrt{\frac{\Delta g}{D_{50}}} \end{cases} \tag{4.28}$$

This formula is developed for sheet-flow conditions (with $\omega_{cr} = 1$). The model shows also satisfactory agreement with the transport data in the ripple regime of Watanabe & Isobe (1990) (with $\omega_{cr} = 0.03$ for $D_{50} = 0.18$ mm and $\omega_{cr} = 0.05$ for $D_{50} = 0.87$ mm) (Dibajnia & Watanabe, 1996).

4.4.5 Dohmen-Janssen (1999)

The model of Dohmen-Janssen (1999) is closely linked to the quasi-steady model of Ribberink (1998). An analytical unsteady sediment transport model is used to calculate the ratio of net sediment transport rate *with* phase lag effects and *without* phase lag effects: the ratio r. This ratio r is used as a phase lag correction factor for the transport rates predicted by the model of Ribberink (1998):

$$\langle q_s \rangle_{\text{Doh}} = r \langle q_s \rangle_{\text{Rib}} \tag{4.29}$$

The model of Ribberink (1998) is a bedload transport model for flat-bed conditions and is valid for different kind of flow conditions: steady, oscillatory, and combined steady-oscillatory flow. The model is based on the assumption that the bed shear stress is the driving force for sediment transport. The basic formula is:

$$\langle \Phi(t) \rangle = \frac{\langle q_{\mathrm{s}}(\mathrm{t}) \rangle}{\sqrt{g \Delta D_{50}^3}} = \left\langle m \left(|\theta'(t)| - \theta_{\mathrm{cr}} \right)^n \frac{\theta'(t)}{|\theta'(t)|} \right\rangle \tag{4.30}$$

with m and n empirical coefficients. The best fit with experimental data was obtained with $m = 11$ and $n = 1.65$. The critical value of the Shields parameter is a function of the non-dimensional grain size D_* according to the relation of Van Rijn (1993).

The phase-lag correction factor r is the ratio of the time-averaged sand transport rates *with* and *without* phase-lag effects. These are called the *real* and the *equilibrium* transport rate respectively. To distinguish between these two an analytical method of Nielsen (1979) is applied. In this approach the sediment concentration $c(z, t)$ is derived from the 1D advection-diffusion equation. By assuming a constant sediment diffusivity ε_{s}, this equation can be solved analytically. The equilibrium concentration profiles can be derived with $\partial c / \partial t = 0$ and the real concentration profiles by solving the full equation. With these concentration profiles and the orbital velocity outside the wave boundary layer, the real and the equilibrium transport rate can be computed. For second-order Stokes waves with an imposed net current, $u(t) = \bar{u} + \hat{u}_1 \cos(\omega t) + \hat{u}_2 \cos(2\omega t)$, the expression for ratio r reads:

$$r = \frac{\bar{u}^3 + \frac{1}{2}\bar{u}\hat{u}_1^2 + \frac{1}{2}\bar{u}\hat{u}_2^2 + \bar{u}\hat{u}_1^2 G_1 + \frac{1}{2}\hat{u}_1^2\hat{u}_2 G_1 + \bar{u}\hat{u}_2^2 G_2 + \frac{1}{4}\hat{u}_1^2\hat{u}_2 G_2}{\bar{u}^3 + \frac{3}{2}\bar{u}\hat{U}_1^2 + \frac{3}{2}\bar{u}\hat{u}_2^2 + \frac{3}{4}\hat{u}_1^2\hat{u}_2} \tag{4.31}$$

with G_1 and G_2 coeffcients depending on the phase lag parameter p:

$$P = \frac{\varepsilon_{\mathrm{s}}\omega}{W_{\mathrm{f}}^2} = \frac{\delta_{\mathrm{s}}\omega}{W_{\mathrm{f}}} \tag{4.32}$$

Dohmen-Janssen (1999) and more recently Dohmen-Janssen *et al.* (2002) compared the models of Ribberink (1998) and Dohmen-Janssen (1999) with a large experimental data set covering a large parameter range in the sheet-flow regime. Dohmen-Janssen (1999) and Dohmen-Janssen *et al.* (2002) conclude that for small phase lags ($P < 0.5$) the net transport rates are predicted well by the quasi-steady model of Ribberink. If phase lags become significant the semi-unsteady model of Dohmen-Janssen (1999) gives better agreement with the data. This model is developed for sheet-flow conditions and is not validated with experimental data in the ripple regime.

4.4.6   Silva (2001)

Silva (2001) developed a general model that predicts the net sediment transport rate in different regimes (plane and rippled beds). The model is based on the work of Dibajnia & Watanabe (1992, 1996). Silva (2001) parameterized this formulation for the following flow conditions:

- waves and a collinear current;

- waves and a current under an oblique angle.

Both second-order Stokes waves and cnoidal waves were considered. The expression for the sediment transport reads:

$$\frac{\langle q_{\mathrm{s}} \rangle}{\sqrt{\Delta g D_{50}^3}} = \alpha \frac{\Gamma}{|\Gamma|^{1-\beta}} \tag{4.33}$$

with α and β empirical coefficients. Silva (2001) calibrated the model on transport data in the sheet-flow regime from Katopodi *et al.* (1994), Koelewijn (1994), Ribberink & Al-Salem (1994), and

Dohmen-Janssen (1999). This resulted in the following values: $\alpha = 0.00019$ and $\beta = 0.55$. The values of Γ, Ω_{c}, Ω_{t}, Ω_{c}', Ω_{t}', ω_{c}, and ω_{t} are determined with the expressions of Dibajnia & Watanabe (1992). According to Silva (2001), the critical value ω_{cr} is a function of the Shields parameter:

$$\hat{\theta}_{2.5} < 0.2 \qquad \omega_{\text{cr}} = 0.035 \tag{4.34a}$$

$$0.2 \leq \hat{\theta}_{2.5} \leq 0.6 \quad \omega_{\text{cr}} = -0.053 + 0.39\hat{\theta}_{2.5} + 0.28\hat{\theta}_{2.5}^2 - 0.161\hat{\theta}_{2.5}^3 \tag{4.34b}$$

$$\hat{\theta}_{2.5} > 0.6 \qquad \omega_{\text{cr}} = -0.408 + 1.367\hat{\theta}_{2.5} - 0.511\hat{\theta}_{2.5}^2 + 0.069\hat{\theta}_{2.5}^3 \tag{4.34c}$$

This expression for ω_{cr} was based the data of Watanabe & Isobe (1990) (ripple regime), Katopodi *et al.* (1994) (sheet-flow), Koelewijn (1994) (sheet-flow), Ribberink & Al-Salem (1994) (sheet-flow and ripple regime), and Dohmen-Janssen (1999) (sheet-flow).

Silva (2001) compared the model with experimental data in the sheet-flow and ripple regime (Watanabe & Isobe, 1990; Ribberink & Al-Salem, 1994). The agreement between the new formulation and the sediment transport data in the ripple regime is not so good: in 20% of the cases the model does not describe correctly the direction of the net transport and only 50% of the computed values are within a factor 2. The results from the new formulation are similar to the results from the original formulation of Dibajnia & Watanabe (1992).

4.5 Unsteady models

Sediment transport is defined as the integral over the water depth of the product of velocity and concentration (or sediment flux, φ):

$$q_{\text{s}} = \int_0^h \varphi \, \mathrm{d}z = \int_0^h u(z,t)c(z,t) \, \mathrm{d}z \tag{4.35}$$

Unsteady models solve this equation by computing the unsteady flow velocity and sediment concentration profiles with the appropriate boundary conditions. Afterwards the sediment transport is averaged over the wave period in order to find the net sediment transport. In this way the wave-related sediment transport and the wave-current interaction is taken into account.

4.5.1 Hydrodynamics

The following subsection is largely based on the work of Holmedal (2002).

Governing equations

Water is considered to be a homogenous isotropic Newtonian fluid. Moreover, the flow field is considered to be incompressible with density ρ and kinematic viscosity ν. Conservation of mass and momentum (Newton's second law) yield the incompressible Navier-Stokes equations, which in absence of external body forces and temperature fields using Cartesian coordinates x, y, z can be written as:

$$\frac{\partial u}{\partial x} + \frac{\partial v}{\partial y} + \frac{\partial w}{\partial z} = 0 \tag{4.36a}$$

$$\frac{\partial u}{\partial t} + u\frac{\partial u}{\partial x} + v\frac{\partial u}{\partial y} + w\frac{\partial u}{\partial z} = -\frac{1}{\rho}\frac{\partial p}{\partial x} + \nu\left(\frac{\partial^2 u}{\partial x^2} + \frac{\partial^2 u}{\partial y^2} + \frac{\partial^2 u}{\partial z^2}\right) \tag{4.36b}$$

$$\frac{\partial v}{\partial t} + u\frac{\partial v}{\partial x} + v\frac{\partial v}{\partial y} + w\frac{\partial v}{\partial z} = -\frac{1}{\rho}\frac{\partial p}{\partial y} + \nu\left(\frac{\partial^2 v}{\partial x^2} + \frac{\partial^2 v}{\partial y^2} + \frac{\partial^2 v}{\partial z^2}\right) \tag{4.36c}$$

$$\frac{\partial w}{\partial t} + u\frac{\partial w}{\partial x} + v\frac{\partial w}{\partial y} + w\frac{\partial w}{\partial z} = -\frac{1}{\rho}\frac{\partial p}{\partial z} + \nu\left(\frac{\partial^2 w}{\partial x^2} + \frac{\partial^2 w}{\partial y^2} + \frac{\partial^2 w}{\partial z^2}\right) \tag{4.36d}$$

with u, v, and w the Cartesian velocity components and p the pressure. It is generally assumed that the Navier-Stokes equations contain all information of the fluid flow. Thus solving (4.36a)-(4.36d) yields the full flow field in the general case. However, due to the complexity and the computational expenses associated with solving the full Navier-Stokes equation, it is normally attempted to find simplified versions of them. These simplifications must be carried out and checked for each individual physical case.

Most flows that occur in nature are turbulent. A turbulent flow field is characterized by three-dimensional velocity and pressure fluctuations and looks somewhat "chaotic" from a visual point of view. In order to extract the mean turbulent flow fields, Osborne Reynolds suggested the following decomposition:

$$u(t) = \bar{u}(t) + u'(t) \tag{4.37a}$$
$$v(t) = \bar{v}(t) + v'(t) \tag{4.37b}$$
$$w(t) = \bar{w}(t) + w'(t) \tag{4.37c}$$
$$p(t) = \bar{p}(t) + p'(t) \tag{4.37d}$$

where $\bar{u}(t)$, $\bar{v}(t)$, and $\bar{w}(t)$ denote the mean turbulent flow field and $u'(t)$, $v'(t)$, and $w'(t)$ the fluctuating turbulent velocity field. The same notation is applied for the pressure field. Substitution of (4.37a)-(4.37d) into the Navier-Stokes equations (4.36a)-(4.36d) and averaging yields the Reynolds-averaged Navier-Stokes equations:

$$\frac{\partial \bar{u}}{\partial t} + \bar{u}\frac{\partial \bar{u}}{\partial x} + \bar{v}\frac{\partial \bar{u}}{\partial y} + \bar{w}\frac{\partial \bar{u}}{\partial z} = -\frac{1}{\rho}\frac{\partial \bar{p}}{\partial x} + \nu\left(\frac{\partial^2 \bar{u}}{\partial x^2} + \frac{\partial^2 \bar{u}}{\partial y^2} + \frac{\partial^2 \bar{u}}{\partial z^2}\right)$$
$$-\frac{\partial \overline{u'^2}}{\partial x} - \frac{\partial \overline{u'v'}}{\partial y} - \frac{\partial \overline{u'w'}}{\partial z} \tag{4.38a}$$

$$\frac{\partial \bar{v}}{\partial t} + \bar{u}\frac{\partial \bar{v}}{\partial x} + \bar{v}\frac{\partial \bar{v}}{\partial y} + \bar{w}\frac{\partial \bar{v}}{\partial z} = -\frac{1}{\rho}\frac{\partial \bar{p}}{\partial x} + \nu\left(\frac{\partial^2 \bar{v}}{\partial x^2} + \frac{\partial^2 \bar{v}}{\partial y^2} + \frac{\partial^2 \bar{v}}{\partial z^2}\right)$$
$$-\frac{\partial \overline{u'v'}}{\partial x} - \frac{\partial \overline{v'^2}}{\partial y} - \frac{\partial \overline{v'w'}}{\partial z} \tag{4.38b}$$

$$\frac{\partial \bar{w}}{\partial t} + \bar{u}\frac{\partial \bar{w}}{\partial x} + \bar{v}\frac{\partial \bar{w}}{\partial y} + \bar{w}\frac{\partial \bar{w}}{\partial z} = -\frac{1}{\rho}\frac{\partial \bar{p}}{\partial x} + \nu\left(\frac{\partial^2 \bar{w}}{\partial x^2} + \frac{\partial^2 \bar{w}}{\partial y^2} + \frac{\partial^2 \bar{w}}{\partial z^2}\right)$$
$$-\frac{\partial \overline{u'w'}}{\partial x} - \frac{\partial \overline{v'w'}}{\partial y} - \frac{\partial \overline{w'^2}}{\partial z} \tag{4.38c}$$

The three additional terms on the right hand side of (4.38a)-(4.38c) act as a stress on the fluid and are called Reynolds stresses or turbulent stresses. The Reynolds stresses must be modeled and each way of modeling gives rise to different turbulence models.

Turbulence models based on the generalized eddy viscosity concept

The oldest method of modeling the Reynolds stresses is the eddy viscosity concept originally introduced by Boussinesq where the turbulent stresses are assumed to be proportional to the mean turbulent velocity gradients. The most common practice today is to use the generalized eddy viscos-

ity concept, which is given as:

$$-\overline{u'^2} = \nu_{\mathrm{t}} \left(\frac{\partial \bar{u}}{\partial x} + \frac{\partial \bar{u}}{\partial x} \right) - \frac{2}{3} k \tag{4.39a}$$

$$-\overline{u'v'} = \nu_{\mathrm{t}} \left(\frac{\partial \bar{u}}{\partial y} + \frac{\partial \bar{v}}{\partial x} \right) \tag{4.39b}$$

$$-\overline{u'w'} = \nu_{\mathrm{t}} \left(\frac{\partial \bar{u}}{\partial z} + \frac{\partial \bar{w}}{\partial x} \right) \tag{4.39c}$$

$$-\overline{v'^2} = \nu_{\mathrm{t}} \left(\frac{\partial \bar{v}}{\partial y} + \frac{\partial \bar{v}}{\partial y} \right) - \frac{2}{3} k \tag{4.39d}$$

$$-\overline{v'w'} = \nu_{\mathrm{t}} \left(\frac{\partial \bar{v}}{\partial z} + \frac{\partial \bar{w}}{\partial y} \right) \tag{4.39e}$$

$$-\overline{w'^2} = \nu_{\mathrm{t}} \left(\frac{\partial \bar{w}}{\partial z} + \frac{\partial \bar{w}}{\partial z} \right) - \frac{2}{3} k \tag{4.39f}$$

with $k = \frac{1}{2}\overline{u'^2} + \frac{1}{2}\overline{v'^2} + \overline{v'^2}$ the turbulent kinetic energy. This turbulent energy can be absorbed by the pressure gradient and therefore application of the generalized eddy viscosity concept reduces turbulence modeling to specifying an appropriate eddy viscosity (Holmedal, 2002). There are in principe three types of eddy viscosity models: zero-equation models, one-equation models, and two-equation models. The zero-equation models can further be divided into four classes: one- and two-layer time-invariant models, one- and two-layer time-dependent models, mixing length models, and models based on the Von Karman momentum integral method. For more details see Janssen (1995) and Holmedal (2002).

Reynolds stress models

An apparently straightforward way of determining the Reynolds stresses is to develop transport equations for the Reynolds stresses, which must be simultaneously solved with the Reynolds-averaged Navier-Stokes equations. The advantage of these Reynolds stress models is that each turbulent stress can be modeled by separate equations. However, in developing these Reynolds stress equations new complicated correlations are introduced. The success of the models is crucially dependent on these correlations. Moreover, the computational effort is larger for the Reynolds stress models than for models based on the generalized eddy viscosity concept. Reynolds stress models have been applied to oscillatory boundary layer flows by e.g. Sheng (1982) and Brørs & Eidsvik (1994).

Large Eddy Simulations

The basic idea behind the Large Eddy Simulations (LES) is that large eddies in a turbulent flow are mainly governed by the physical boundaries, while the small-scale turbulence is mainly independent of the physical boundaries. Thus, it is natural to compute the large three-dimensional time-dependent turbulent structures directly from the Navier-Stokes equations and to impose a turbulence model for the smaller turbulent scales. The advantage of LES models over the turbulence models is a more realistic description of the flow: realizations of the three-dimensional time-dependent large-scale turbulent flow are obtained. However, the problem of applying LES on the sea bed boundary layer is that rough sea beds are difficult to handle. Large Eddy Simulations of the oscillatory boundary layer have been performed by Vittori & Armenio (2000).

Direct Numerical Simulations

Since the Navier-Stokes equations are assumed to contain all physical information of the flow, turbulence can be calculated directly from these equations without any modeling at all. The turbulence is introduced in the calculations either by a random perturbation of the initial flow field or by random

perturbations of the physical boundary conditions. These calculations require a resolution of (ideally) all turbulent spacial and temporal scales. This makes the calculations very computational expensive and presently this method can only be applied on flows with moderate Reynolds numbers, simple geometries, and smooth surfaces hoping that these kind of simulations provide physical information which is useful for rough sea beds as well. Scandura *et al.* (2000) carried out simulations of oscillatory flow over steep ripples, solving the full three-dimensional Navier-Stokes equations in curvilinear coordinates. The simulations are limited to the laminar regime; flow instabilities due to the ripples were visualized and compared with simpler theories.

Discrete vortex models

A special type of models to describe the flow above ripples are the discrete vortex models. These models are based on the Poisson equation for the flow and the convection-diffusion equation for the vorticity. A complete numerical solution of these equations is not feasible for high Reynolds numbers and the discrete-vortex models have therefore been developed to make it possible to obtain approximate solutions. The main assumption behind this method is that vorticity can be represented by a number of discrete (point) vortices. Vorticity is generated in the vicinity of the boundary and then transported by the flow velocity. The discrete vortex model does not make a prediction about the structure of the near-bed flow. It is assumed that the outer flow region (discrete vortex model) can be decoupled from the near-bed region (oscillatory boundary model), which requires the boundary layer to be small compared with the ripple height. According to Block *et al.* (1994) the thickness of the boundary layer may be expected to lie in the range 0.1-0.2η for the parameter ranges corresponding to equilibrium ripples. To this extent the decoupling of the discrete model and the boundary layer model is justified.

One of the first discrete-vortex models was developed by Longuet-Higgins (1981). This high Reynolds number model succeeded in capturing most of the dynamics of vortex shedding. An analytical discrete-vortex model is developed by Block *et al.* (1994). Block *et al.* (1994) showed that the phase angle of eddy shedding during the wave cycle depends on the ratio d_{o}/λ. In simulations of regular waves above a very fine sediment bed, Block *et al.* (1994) found that the lee-slope eddy was shed (and moved over the ripple crest) after flow reversal for $d_{\mathrm{o}}/\lambda = 1.6$ and before flow reversal for $d_{\mathrm{o}}/\lambda = 2.6$, in accordance with their experimental observations. For larger values of d_{o}/λ and correspondingly smaller ripple steepnesses, eddy shedding started to break down and ultimately the simple discrete-vortex model could not be used in this low-rippled very-rough bed regime. Hansen *et al.* (1994), Perrier (1996), and Malarkey (2001) have developed numerical discrete-vortex models.

4.5.2   Sediment dynamics

Advection-diffusion equation

The equation for the unsteady sediment concentration can be found from the mass balance of sediment assuming that the sediment can be transported by advection as well as diffusion. It is assumed that these two processes are independent and can be superimposed linearly. The advection-diffusion equation reads:

$$\frac{\partial c}{\partial t} + u_{\mathrm{s}}\frac{\partial c}{\partial x} + v_{\mathrm{s}}\frac{\partial c}{\partial y} + w_{\mathrm{s}}\frac{\partial c}{\partial z} = \varepsilon_{\mathrm{m}}\left(\frac{\partial^2 c}{\partial x^2} + \frac{\partial^2 c}{\partial y^2} + \frac{\partial^2 c}{\partial z^2}\right) \tag{4.40}$$

with u_{s}, v_{s}, and w_{s} the velocity components of sediment particles and ε_{m} the molecular sediment diffusivity, which is assumed to be homogeneous and isotropic. Similar to the Navier-Stokes equations, the parameters in the advection-diffusion equation can be split up into mean turbulent and fluctuating

turbulent components. Substitution into (4.40) and Reynolds averaging yields:

$$\frac{\partial \bar{c}}{\partial t} + \bar{u}_{\text{s}} \frac{\partial \bar{c}}{\partial x} + \bar{v}_{\text{s}} \frac{\partial \bar{c}}{\partial y} + \bar{w}_{\text{s}} \frac{\partial c}{\partial z} = \varepsilon_{\text{m}} \left(\frac{\partial^2 \bar{c}}{\partial x^2} + \frac{\partial^2 \bar{c}}{\partial y^2} + \frac{\partial^2 \bar{c}}{\partial z^2} \right)$$
$$- \frac{\partial \overline{c' u'_{\text{s}}}}{\partial x} - \frac{\partial \overline{c' v'_{\text{s}}}}{\partial y} - \frac{\partial \overline{c' w'_{\text{s}}}}{\partial z} \tag{4.41}$$

The three terms that appear on the right-hand side of (4.41) can analogous to the Boussinesq hypothesis for the Reynolds stresses be described with the following expressions:

$$-\overline{c' u'_{\text{s}}} = \varepsilon_{\text{s}} \frac{\partial \bar{c}}{\partial x} \tag{4.42a}$$

$$-\overline{c' v'_{\text{s}}} = \varepsilon_{\text{s}} \frac{\partial \bar{c}}{\partial y} \tag{4.42b}$$

$$-\overline{c' w'_{\text{s}}} = \varepsilon_{\text{s}} \frac{\partial \bar{c}}{\partial z} \tag{4.42c}$$

where ε_{s} is the turbulent sediment diffusivity, which is closely related to the eddy viscosity.

Lagrangian particle tracking

If a significant part of the turbulence is actually resolved in the hydrodynamical model it is possible to use a Lagrangian formulation, where the individual grains are followed. The change in a particle's position is found from time t to time $t + \Delta t$ as the combination of convection and settling of the particle:

$$x(t + \Delta t) = x(t) + u_{\text{s}}(t) \Delta t \tag{4.43a}$$
$$y(t + \Delta t) = y(t) + v_{\text{s}}(t) \Delta t \tag{4.43b}$$
$$z(t + \Delta t) = z(t) + w_{\text{s}}(t) \Delta t \tag{4.43c}$$

This formulation of the behaviour of the suspended particles is well suited for situation in which convection dominates the sediment motion; the advection-diffusion equation (4.41) can be more appropriate if turbulent diffusion is dominant. According to Hansen *et al.* (1994) the convection transport is dominant in the entire flow domain except in the boundary layer that forms along the ripple surface. This situation is in many ways analogous to the problem of the vorticity generated in the boundary layer: the sediment can only be entrained into the flow from the ripple surface, and it has to pass the near-bed boundary layer by turbulent diffusion before it reaches the region where convection is dominant. The sediment concentration in the boundary layer can then be modeled with the advection-diffusion equation. Lagrangian particle tracking is used in the discrete vortex models of Block *et al.* (1994), Hansen *et al.* (1994), and Perrier (1996).

4.5.3 Discussion unsteady model types

Since it is assumed that the Navier-Stokes equations contain all physical information of the flow, LES and especially DNS seem to be the most preferable approaches to describe the hydrodynamics over a rippled bed. However, the problem of applying LES and DNS on the seabed boundary layer is that rough sea beds are difficult to handle (Holmedal, 2002). DNS can only be applied on flows with moderate Reynolds number and simple geometries (Holmedal, 2002). Moreover, the calculations are very computational expensive. Hence, these model approaches are considered not to be appropriate for the present research.

The major drawback against the discrete-vortex method is that it is essentially inviscid and therefore only a part of the turbulent diffusion process can be simulated directly. Therefore sand can not be entrained to sufficient heights above the bed (Block *et al.*, 1994).

It is still not clear whether turbulence-closure models are able to represent coherent vortex dynamics realistically. Perrier (1996) compared the results of a discrete-vortex model and a Reynolds stress closure model and found that both models simulated the formation and shedding of vortices realistically. Perrier (1996) also found that higher-order Reynolds stress models should provide more accurate results than two-equation models. However, Andersen (1999) simulated the formation and shedding of vortices realistically with a two-equation k-ω closure model. Furthermore, turbulence-closure models require less computation time than LES and DNS and are more attractive since they have a longer validation and refining history. It is important to notice that the real bottleneck in sand transport modeling over ripples is not the description of the hydrodynamics, but the sand transport description itself. Therefore, a sophisticated description of the hydrodynamics may be important, but it does not solve all uncertainties in computing the sand transport rate.

It is therefore concluded that the most appropriate model approach for the present research is a turbulence-closure model for the hydrodynamics and the advection-diffusion equation for the sediment dynamics. Such transport models are described in the following sections.

4.5.4   Assumptions in sediment transport models

Sediment transport can be described with the Reynolds-averaged Navier-Stokes equations and the advection-diffusion equation. To simplify the solutions the following assumptions are common in most of these sediment transport models.

1. Flow and sediment transport over ripples with primarily 2D geometries is a 2DV (x,z) problem; the Navier-Stokes and advection-diffusion equation in y-direction can be omitted.

2. The velocity in the Navier-Stokes equation is that of the fluid, while the velocity in the advection-diffusion equation is the velocity of the sediment particles. It is generally assumed that the velocity of the sediment particles in x-direction equals the fluid velocity. In z-direction it is assumed that the only difference between the sediment and fluid velocity is due to the sediment fall velocity W_f. This results in:

$$u_\mathrm{s}(t) = u(t)$$
$$w_\mathrm{s}(t) = w(t) - W_\mathrm{f}$$

   where the sediment fall velocity is assumed to be constant.

3. The molecular viscosity is much smaller than the turbulent viscosity, $\nu_\mathrm{m} << \nu_\mathrm{t}$. The same applies for the sediment diffusivity: $\varepsilon_\mathrm{m} << \varepsilon_\mathrm{s}$.

The resulting equations are:

$$\frac{\partial u}{\partial x} + \frac{\partial w}{\partial z} = 0 \tag{4.44}$$

$$\frac{\partial u}{\partial t} + u\frac{\partial u}{\partial x} + w\frac{\partial u}{\partial z} = -\frac{1}{\rho}\frac{\partial p}{\partial x} + 2\frac{\partial}{\partial x}\left(\nu_\mathrm{t}\frac{\partial u}{\partial x}\right) + \frac{\partial}{\partial z}\left(\nu_\mathrm{t}\left(\frac{\partial u}{\partial z} + \frac{\partial w}{\partial x}\right)\right) \tag{4.45}$$

$$\frac{\partial w}{\partial t} + u\frac{\partial w}{\partial x} + w\frac{\partial w}{\partial z} = -\frac{1}{\rho}\frac{\partial p}{\partial z} + 2\frac{\partial}{\partial z}\left(\nu_\mathrm{t}\frac{\partial w}{\partial z}\right) + \frac{\partial}{\partial x}\left(\nu_\mathrm{t}\left(\frac{\partial u}{\partial z} + \frac{\partial w}{\partial x}\right)\right) \tag{4.46}$$

$$\frac{\partial c}{\partial t} + \frac{\partial}{\partial x}(uc) + \frac{\partial}{\partial z}((w - W_\mathrm{f})c) = \frac{\partial}{\partial x}\left(\varepsilon_\mathrm{s}\frac{\partial c}{\partial x}\right) + \frac{\partial}{\partial z}\left(\varepsilon_\mathrm{s}\frac{\partial c}{\partial z}\right) \tag{4.47}$$

4.5.5   Boundary conditions

The boundary conditions for the solution of the Navier-Stokes equations are:

$$\text{at } z = z_0 \quad u(t) = 0 \qquad , w(t) = 0 \tag{4.48a}$$

$$\text{at } z = z_\infty \quad u(t) = u_\infty(t) , w(t) = w_\infty(t) \tag{4.48b}$$

with z_0 the level where the velocity is assumed to be zero ($= k_s/30$) and z_∞ a specified level just outside the boundary layer. It is thus assumed that the orbital velocity equals zero at $z = z_0$, which is called the "no-slip condition". At the top of the boundary layer the orbital velocity equals its free stream velocity. The boundary conditions for the advection-diffusion equation are:

$$\text{at } z = z_b \quad c(t) = c_b(t) \quad \text{or} \quad \frac{\partial c(t)}{\partial z} = \left.\frac{\partial c(t)}{\partial z}\right|_{z=z_b} \tag{4.49a}$$

$$\text{at } z = z_\infty \quad \phi(t) = w_s c(t) + \varepsilon_s \frac{\partial c(t)}{\partial z} = 0 \tag{4.49b}$$

where z_b is the reference level for the bottom boundary condition. There are two types of boundary conditions: a "reference concentration" type and a "pick-up function" type. In the first type it is assumed that the bed concentration reacts instantaneously to changes in the flow velocity (usually through the Shields parameter), $c_b = f(\theta)$. In a pick-up function it is assumed that the upward sediment flux or pick-up rate rather than the concentration reacts instantaneously to changes in the flow velocity:

$$\left.\frac{\partial c(t)}{\partial z}\right|_{z=z_b} = -\frac{w_s}{\varepsilon_s} c_b(t) \tag{4.50}$$

where c_b can be derived using a reference concentration boundary condition. With a pick-up function boundary condition, the concentration at the reference level may be larger than given by the expression for the reference concentration due to grains settling from above. Hagatun & Eidsvik (1986) propose a compromise method to take into account the possibility of a higher reference concentration at low values of the bed shear stress due to grains settling from above. In this method the reference concentration $c_b(\theta)$ is determined as the maximum of the concentration at time t and the concentration one time-step Δt earlier at the level $z = z_b + \Delta t w_s$.

The advection-diffusion equation describes the suspended sediment concentration. Therefore, the reference level z_b is often assumed to be at the lower limit of the suspended load layer, which is approximately two times the sediment grain size ($z_b = 2D_{50}$). The bedload transport taking place between the zero-velocity level $z = z_0$ and $z = 2D_{50}$ is then described in a quasi-steady manner with a transport formula derived for steady flows. However, the use of bedload transport formula is not fully consistent with the choice of a fixed reference level (the lower limit of the suspended load layer). Therefore, it may be more appropriate to exclude the bedload transport and compare the measured value of net transport with the predicted value of suspended sediment transport (Davies & Li, 1997).

The choice of the bed boundary condition for the advection-diffusion equation is a very arbitrary one with great consequences for the transport rate. This especially accounts for rippled beds with strong time- and space-varying flow conditions. There is not a "correct" way of dealing with this and it is one of the bottlenecks in modeling sediment dynamics.

4.5.6 Sediment-flow interaction

In sediment transport models it is often assumed that the amounts of suspended sediment are so small that they have no influence on the flow structure. For the flow far away from the bed where the concentration is small this might be reasonable. However, the near-bed sediment concentration is often high enough to violate this assumption. There are in principle two methods to take sediment-flow interaction into account. The first is by modifying the existing models for the effects of the high sediment concentration. The second more fundamental one is by considering the flow to consist of two phases: a solid and a fluid phase. For these two phases the mass and momentum balance equation are solved separately. This method results in very complex sediment transport models with time-consuming computations. Therefore, an intermediate method exists where the flow is divided into two or more layers with different significance of sediment-flow interaction. For sediment transport in the ripple regime, the first method to take sediment-flow interaction into account is sufficient considering the amounts of sediment in suspension.

Because of the decreasing sediment concentration with height, a density gradient exists in the vertical direction that introduces buoyancy forces into the flow. This stratification inhibits the turbulent transport of mass and momentum. Stratification is characterized by the *flux* Richardson number R_i, which indicates the importance of buoyancy and is defined as the ratio of gravity to inertia forces:

$$R_i = -\frac{g}{\rho}\frac{w'\rho'}{u'w'\frac{\partial u}{\partial z}} = -\frac{g}{\rho}\frac{\varepsilon_s\frac{\partial\rho}{\partial z}}{\nu_t\left(\frac{\partial u}{\partial z}\right)^2} \tag{4.51}$$

The turbulent fluctuations of the density are caused by the turbulent fluctuations of the concentration. A different number can also be used, which is called the *gradient* Richardson number:

$$R_g = -\frac{g}{\rho}\frac{\frac{\partial\rho}{\partial z}}{\left(\frac{\partial u}{\partial z}\right)^2} = \sigma_c R_i \tag{4.52}$$

with σ_c the Schmidt number ($= \nu_t/\varepsilon_s$). For situations where $\partial\rho/\partial z < 0$ (decreasing density caused by decreasing concentration with height) the Richardson number is positive and the flow is stably stratified. If $\partial\rho/\partial z > 0$ the Richardson number is positive and the stratification is unstable. Stable stratification inhibits the turbulent transport of mass and momentum, while unstable stratification enhances this transport. In case of a constant density over height ($R_i = R_g = 0$), buoyancy and stratification are absent. For zero-equation models this so-called turbulence damping is accounted for by modification of the eddy viscosity and the sediment diffusivity. In more complex one- and two-equation models the transport equations for turbulent parameters contain buoyancy terms.

In high sediment concentrations, the settling velocity of the sediment will be different than for a single particle. Based on simple continuity considerations it can be shown that if sediment is settling in high concentrations the downward sediment flux must be compensated by an upward flux of water. This upward flow reduces the settling velocity of sediment particles, which is called hindered settling. This phenomenon can be taken into account using the expression derived by Richardson & Zaki (1954):

$$w_{hs} = (1 - c)^\gamma\, w_s \tag{4.53}$$

where w_{hs} is the settling velocity due to hindered settling. The exponent γ varies between 2.3 and 4.6 depending on the Reynolds number.

4.6   1DV turbulence-closure models

4.6.1   Point Sand model

Uittenbogaard *et al.* (2000) developed the 1DV Point Sand model, which is a numerical simulation of wave-current driven sediment transport above plane beds. The model has the following properties.

- One-equation k turbulence-closure or two-equation k-ϵ turbulence-closure with ϵ the turbulent dissipation rate.

- $\nu_t = \beta\varepsilon_s$ with β a user-defined parameter.

- Turbulence damping included.

- The reference (mass) concentration of Zyserman & Fredsøe (1994) is used:

$$c_b(t) = \frac{0.331\left(\theta - \theta_{cr}\right)^{1.75}}{1 + \frac{0.331}{c_m}\left(\theta - \theta_{cr}\right)^{1.75}} \quad \text{at} \quad z = 2D_{50} \tag{4.54}$$

in which the maximum concentration c_{m} has a value of 0.32 that deviates from the original value. The critical Shields value is determined using the method of Van Rijn (1993) where $\theta_{\mathrm{cr}} = f(D_*)$. It is also possible to define a pick-up function at $z = 2D_{50}$ based on this reference concentration:

$$\left.\frac{\partial c}{\partial z}\right|_{z=z_{\mathrm{b}}} = -\frac{w_{\mathrm{s}}}{\varepsilon_{\mathrm{s}}} c_{\mathrm{b}}(t) \tag{4.55}$$

Hindered settling is accounted for using the expression proposedby Richardson & Zaki (1954):

$$W_{\mathrm{f}} = \left(1 - \frac{c}{c_{\mathrm{s}}}\right)^5 W_{\mathrm{f,0}} \tag{4.56}$$

with c the volumetric concentration and $c_{\mathrm{s}} = 0.65$ the maximum volume fraction of solids in a non-cohesive porous bed. The particle fall velocity $W_{\mathrm{f,0}}$ is computed according to the formula of Van Rijn (1993).

- Recently (Hassan, 2003), the bed-load formula of Engelund & Fredsøe (1976) was implemented in the Point Sand model, see Equations (4.63) and (4.64).

The direction of the waves with respect to the current is arbitrary. Orbital motions are solved for each spectral component and the waves are assumed spatially periodic. Both the mean flow and the orbital motions are solved over the entire water depth. The effect of waves on the mean velocity profile is modeled by taking wave-current interaction into account.

Validation

Sistermans (2002) compared his concentration and transport data with results from the Point Sand model. The ripple effects were taken into account through an increased bed roughness related to the ripple dimensions. This model, originally developed for the simulation of sediment transport above flat beds, reproduced the time-averaged concentration and velocity profiles above ripples reasonably. However, the measured negative wave-related transport (thus against the direction of wave propagation) was not reproduced by the model. Therefore, Sistermans (2002) concludes that the Point Sand model does not simulate correctly the time-dependent sediment transport over a rippled bed.

4.6.2 UWB model

Description

Davies & Li (1997) developed the original UWB (University of Wales, Bangor) model capable of describing sediment transport for unsteady flow above a plane bed. This model is later extended to cover the ripple regime as well (Davies & Thorne, 2002). The main features of the flat bed model are:

- One-equation turbulent kinetic energy (k) closure.

- $\nu_{\mathrm{t}} = \varepsilon_{\mathrm{s}}$.

- Turbulence damping included.

- The reference concentration of Engelund & Fredsøe (1976) modified by Fredsøe *et al.* (1985) is used:

$$c_{\mathrm{b}} = \frac{0.65}{(1 + 1/\lambda)^3} \qquad \text{at} \quad z = 2D_{50} \tag{4.57}$$

where the so-called linear concentration λ is given by:

$$\lambda = \left(\frac{|\theta| - \theta_{\mathrm{cr}} - \pi p_*/6}{0.027 \, |\theta| \, s} \right)^{0.5} \quad \text{for} \quad |\theta| > \theta_{\mathrm{cr}} + \pi p_*/6 \tag{4.58}$$

$$\lambda = 0 \quad \text{for} \quad |\theta| \le \theta_{\mathrm{cr}} + \pi p_*/6 \tag{4.59}$$

and p_* is defined by:

$$p_* = \left[1 + \left(\frac{\pi/6}{|\theta| - \theta_{\mathrm{cr}}} \right)^4 \right]^{-1/4} \tag{4.60}$$

with $s = \rho_{\mathrm{s}}/\rho$ and $\theta_{\mathrm{cr}} = 0.045$. This includes the settling correction from Hagatun & Eidsvik (1986).

- The instantaneous bedload transport rate is estimated by Li & Davies (1996) using the formula of Meyer-Peter & Müller (1948):

$$q_{\mathrm{b}} = 8 \left(|\theta| - \theta_{\mathrm{cr}} \right)^{1.5} \sqrt{\Delta g D_{50}^3} \frac{\theta}{|\theta|} \quad \text{for} \quad |\theta| > \theta_{\mathrm{cr}} \tag{4.61a}$$

$$q_{\mathrm{b}} = 0 \quad \text{for} \quad |\theta| \le \theta_{\mathrm{cr}} \tag{4.61b}$$

where $\theta_{\mathrm{cr}} = 0.045$.

In the new model two layers are distinguished: a lower vortex-dominated region and an upper layer. The changeover level corresponds to two ripple heights above the (undisturbed) mean bed level. In the upper layer the model reverts to the standard turbulence-closure formulation. In the lower layer an analytical near-bed sub-model represents the processes of vortex shedding and the associated entrainment of sediment at times of flow reversal. A distinction is made between steep ripples (with a steepness greater than about 0.12) and flat ripples. The latter case where coherent motions are less pronounced is treated by running the "standard" flat bed model with an enhanced roughness: $k_{\mathrm{s}} = 25\eta^2/\lambda$. If the ripple dimensions are not known from observation they are calculated using an adjusted formulation of Wiberg & Harris (1994).

In the "rippled-bed sub-model" the eddy viscosity is used to represent ripple-related vortices. This height-independent strongly time-varying eddy viscosity has maxima just ahead of times of flow reversal. Its mean value is determined using the formula proposed by Nielsen (1992) for very rough beds. In the continuity equation for suspended sediment, the diffusivity is taken as about 4 times the eddy viscosity as suggested by Nielsen (1992) on the basis of experimental data for rippled beds. This factor is needed in the vortex-dominated layer to account for the 2-D and 3-D spatial-temporal correlations between high concentrations and locally upward velocities during the vortex shedding process. The bottom boundary condition in the rippled-bed model is a strongly time-varying pick-up function, which represents sediment entrainment associated with the vortex shedding process. This condition is imposed at the ripple crest level, the mean value of the pick-up function being based on empirical reference concentration formula for ripples from Nielsen (1986), see (3.5). Data from the Delta Flume (Thorne et al., 2002) has been used to define the phase angle of sediment pick-up during the wave cycle. According to the data, peak suspended concentrations at the ripple crest level occur just ahead of flow reversal (about midway between maximum velocity and reversal in free stream) and the phase of sediment pick-up has been defined accordingly. The above procedures for the wave alone have also been extended for combined wave and current flow, see Davies & Thorne (2002). There is no bedload formulation included in the rippled-bed model.

Validation

Davies & Thorne (2002) compared the above-described model with ABS (Acoustic Back Scatter) concentration profile data from the Delta Flume at Delft Hydraulics (Thorne et al., 2002). On

the basis of an analysis of horizontally-averaged ABS concentration data, Davies & Thorne (2002) conclude that it seems justifiable to represent sediment in suspension above ripples using a 1DV model. Furthermore, Davies & Thorne (2002) conclude that the model makes reasonable predictions of the ripple dimensions, the reference concentration, and mean concentration profiles. In addition, intra-wave processes were modeled satisfactory.

4.6.3 UT model

This 1DV boundary layer flow and transport model for unsteady flow was developed by Ribberink & Al-Salem (1991a). Application of this UT (University of Twente) model is limited to plane bed conditions or to conditions with (wave-induced) ripple dimensions that are considerably smaller than the horizontal excursion length of the oscillatory flow. In the latter case, the influence of ripples is taken into account by imposing a larger bed roughness, e.g. $k_\mathrm{s} = 25\eta^2/\lambda$. Furthermore, the UT model has the following characteristics.

- Mixing length turbulence-closure. Using the Prandtl mixing-length theory with mixing-length $l = \kappa z$ as turbulence-closure, the following time-dependent eddy viscosity follows:

$$\nu_\mathrm{t} = \kappa^2 z^2 \left| \frac{\partial u}{\partial z} \right| \tag{4.62}$$

  with κ the Von Karman constant which is equal to 0.4.

- $\nu_\mathrm{t} = \beta \varepsilon_\mathrm{s}$ with β a user-defined parameter.

- Turbulence damping not included.

- The reference concentration formulas of Engelund & Fredsøe (1976) modified by Fredsøe *et al.* (1985) and Zyserman & Fredsøe (1994) are implemented. No settling correction is included.

- There is no bedload formulation included in the model framework.

Validation

The UT model is not validated with experimental data in the ripple regime.

4.7 2DV turbulence-closure models

4.7.1 DTU model

The Technical University of Denmark (DTU) developed a 2DV model to describe the sediment transport above ripples for unsteady flow (Andersen, 1999). The computational model consists of a flow, sediment transport, and morphological module. Therefore, it is possible to compute with "live" (moving) ripples rather than fixed ripples. Furthermore, the model has the following features.

- Two-equation k-ω turbulence-closure with ω the specific turbulent dissipation rate.

- $\nu_\mathrm{t} = \varepsilon_\mathrm{s}$.

- Turbulence damping not included.

- The reference concentration at $z = 2D_{50}$ is described by the expression of Engelund & Fredsøe (1976) modified by Fredsøe *et al.* (1985). The sloping bed is taken into account through the critical Shields parameter with a strong down-slope flux if the bed slope is larger than the angle of repose.

- The bedload is described using the Engelund & Fredsøe (1976) formulation:

$$\Phi_{\mathrm{b}} = \alpha \frac{\pi}{6} p \left[\sqrt{\theta} - 0.7\sqrt{\theta_{\mathrm{cr}}} \right] \tag{4.63}$$

with α a coefficient that relates the near-bed flow velocity and the friction velocity ($\simeq 10$) and p the probability of grains in transport:

$$p = \left[1 + \left(\frac{\frac{\pi}{6}\mu_{\mathrm{d}}}{\theta - \theta_{\mathrm{cr}}} \right)^4 \right]^{-0.25} \tag{4.64}$$

with μ_{d} the dynamic friction coefficient ($= \tan\phi$ with ϕ the angle of repose).

According to Andersen (1999), the k-ω model is similar to the popular k-ϵ model, but has two improvements: i)it is possible to integrate through the viscous sub-layer without dubious damping functions, thus avoiding the use of wall-functions and ii)the model is known to perform better in flows with strong adverse pressure gradients, which is exactly the case for the wave boundary layer. Furthermore, the boundary conditions on the bed for k and ω are simple making it possible to account for both smooth and rough bed conditions (Andersen & Fredsøe, 1999).

Validation

The DTU model has not been validated with experimental data in the ripple regime.

4.7.2   IMAR model

The 2DV model developed by IMAR is capable of computing the unsteady flow and suspended transport above plane and rippled beds (Huyn Thanh & Temperville, 1990; Huyn Thanh *et al.*, 1994; Silva, 2001). The main features of the IMAR model are:

- Two-equation k-L closure with L the characteristic length scale of the large vortices.

- $\nu_{\mathrm{t}} = \frac{4}{3}\varepsilon_{\mathrm{s}}$.

- Turbulence damping included.

- The reference concentration of Engelund & Fredsøe (1976) modified by Fredsøe *et al.* (1985) is used. This includes the settling correction from Hagatun & Eidsvik (1986).

- There is no bedload formulation included in the model framework.

Validation

The IMAR model has been validated with experimental data of Ribberink & Al-Salem (1989) (concentrations), Sato *et al.* (1984) (hydrodynamical), and Silva *et al.* (1999) (hydrodynamical) in the ripple regime.

4.7.3   SINTEF model

SINTEF developed a 2DV model based on the Reynolds-averaged Navier-Stokes equations and the advection-diffusion equation to study sediment transport over rippled beds under both steady and unsteady flow (Brørs, 1999; Utnes & Meling, 1999; Eidsvik, 2001). The model contains a morphological module. Furthermore, the model has the following characteristics.

- Two-equation k-ϵ turbulence-closure.

- $\nu_{\mathrm{t}} = \varepsilon_{\mathrm{s}}$.

Current alone			
$H_s = 0$ m, $\hat{u} = 0$ ms^{-1}			
Current+Waves 1 & 2		**Current+Waves 3 & 4**	
1) $H_s = 0.5$ m, $T = 5$ s,		3) $H_s = 2.0$ m, $T = 7$ s,	
$\hat{u} = 0.255$ ms^{-1}		$\hat{u} = 1.207$ ms^{-1}	
2) $H_s = 1.0$ m, $T = 6$ s,		4) $H_s = 3.0$ m, $T = 8$ s,	
$\hat{u} = 0.568$ ms^{-1}		$\hat{u} = 1.879$ ms^{-1}	
depth-mean $\bar{u}$ (m/s)	k_s (m)	depth-mean $\bar{u}$ (m/s)	k_s (m)
0.1	0.1	0.1	flat
0.3	0.1	0.3	flat
0.5	0.1	0.5	flat
0.6	0.1	0.6	flat
0.7	0.1	0.7	flat
0.8	0.1	0.8	flat
1.0	0.1	1.0	flat
1.2	0.08	1.2	flat
1.5	0.06	1.5	flat
1.8	0.03	1.8	flat
2.0	flat	2.0	flat

Table 4.1: Model input for the intercomparison of the different research models (Davies *et al.*, 2002).

- Turbulence damping included.

- The reference concentration of Engelund & Fredsøe (1976) modified by Fredsøe *et al.* (1985) is imposed at $z = 2D_{50}$ with $\theta_{cr} \approx 0.05$.

- The bedload is described with the empirical formula of Meyer-Peter & Müller (1948).

Validation

The SINTEF model has not been validated with experimental data in the ripple regime.

4.8 Comparison models

Davies *et al.* (2002) intercompared research and practical sediment transport models and compared models with field data. The term research model denotes a model that represents many of the detailed physical processes involved in sediment transport by waves and currents including intra-wave processes. Practical models are simpler prediction schemes that either do not resolve the spatial and temporal structure of the velocity and concentration fields or, if they do so, use simplified and prescriptive approaches for this purpose.

4.8.1 Intercomparison of research models

Davies *et al.* (2002) intercompared seven research for defined ranges of (co-linear) wave and current conditions above a uniform sediment bed with $D_{50} = 0.25$ mm including the (above-described) UWB model, the UT model, the DTU model, and the SINTEF model. Each model had to calculate the sediment flux including the wave-related component of the suspended load transport for defined conditions. Table 4.1 shows the prescribed parameter settings for the intercomparison task. For flat beds $k_s = 2.5D_{50}$. The UWB and UT model could deal with all prescribed wave and current conditions. The DTU model was only run for a limited number of cases in which the bed was considered/expected to comprise ripples of sufficient steepness. The SINTEF model was run over the parameter ranges including the currents alone and the currents combined with Waves 1 and 2.

In case of plane beds, the agreement between the predicted net transport rates was well within one order of magnitude. In addition, the relative behaviour of the models was very similar. The disagreement exhibited by the various models in the rippled-bed cases is substantial, up to two orders of magnitude in some cases. Particularly disturbing is the fact that the two 2DV models (DTU and SINTEF) showed such marked disagreement. Davies *et al.* (2002) suggest that this may be connected with the different ripple shapes used in the respective models for the given bed roughness. As far as the 1DV models (UWB and UT) are concerned, the difference is almost certainly due to the different treatment of the near-bed flow and specifically due to the height of implementation of the reference concentration. Differences between the various turbulence-closure schemes are unlikely to have accounted for the overall discrepancy in the absolute transport rates in the rippled-bed cases. In a relative sense the behaviour of the models was rather different for the currents alone, but became more closely similar as the wave height (velocity amplitude) increased.

4.8.2   Intercomparison of practical models

Davies *et al.* (2002) also intercompared five practical models including the model from Silva (2001) and two research models including the UWB model. The same waves and currents were used as in the intercomparison of the research models, see Table 4.1. However, the waves and currents were combined perpendicularly. The modeling was now focussed on the current-related transport component in longshore direction. Moreover, there was the potential for the suspended grain size to vary from run to run due to the mixed bottom grain size, $D_{50} = 0.25$ mm and $D_{90} = 0.50$ mm. The bed roughness was prescribed as indicated in Table 4.1 except that the roughness of the beds denoted "flat" was taken as $k_s = 0.02$ m, representative for field conditions. Furthermore, the waves were supposed to be irregular (JONSWAP spectrum).

For plane beds, the current-related longshore transport rates predicted by the models varied by a factor 10 to 30 in the individual case (somewhat higher than the equivalent variation found for the research models). For rippled beds, the variation was in the range 50 to 200. The largest transport rates were predicted by the Silva (2001) model. The UWB model predicts relatively low transport rates in the cases involving weaker currents and smaller waves for which bedload was the dominant transport mode. The underlying reason for these low predictions of the bedload was the strict use by the model of skin friction concepts derived from laboratory work, which may have underestimated the skin friction and hence the bedload in the field conditions of present interest (Davies *et al.*, 2002).

4.8.3   Intercomparison of practical models with field data

Davies *et al.* (2002) did not only compare the seven practical models for a fictive case, but also for five field data sets: Madsen *et al.* (1993), Kroon (1994) and Wolf (1997), Whitehouse *et al.* (1996), Whitehouse *et al.* (1997), and Williams *et al.* (1997). Here the results show that the suspended sediment concentrations were predicted within a factor 2 of the measured values in 13% to 48% of the cases considered and within a factor 10 in 70% to 83% of the cases (UWB model 15% and 72% respectively). The UWB model tends to overpredict high concentrations and underpredict low concentrations. Estimates of the longshore (current-related) component of suspended sediment transport made by the five models yielded agreement within a factor 2 of the measured values in 22% to 66% of cases and within a factor 10 in 77% to 100% of cases (UWB model 66% and 100% respectively; the Silva (2001) model 55% and 88% respectively). The UWB and Silva (2001) model produced generally good predictions, though with an underprediction for high values of H_s/h.

4.8.4   General conclusions intercomparison task

Although substantial differences have been found between the absolute magnitudes of the transport rates predicted by different models, it is important to note that it is not only the *absolute* predictions that are important in sediment transport research. From the point of view of the morphological modeler, it is important that a transport model shows the correct behaviour i)as a function of input

parameters and ii)over a wide range of conditions involving several orders of magnitude in the transport rate. Since there is more agreement in the relative behaviour of many of the models than in their ability to produce the same absolute magnitudes for the transport rate, the results of the comparison could be viewed as rather encouraging from the point of view of morphological modelers (Davies *et al.*, 2002). Davies *et al.* (2002) conclude that the emphasis in future work should be directed towards improved models for rippled-bed conditions.

4.9 Discussion 1DV approach

This section deals with the question: *is it possible to model sediment transport above wave-induced ripples with a 1DV model?* Let us first consider what the requirements are for a horizontally uniform flow, i.e. $u(z,t)$ instead of $u(x,z,t)$. The first requirement for horizontal uniformity is that the u_∞ is horizontally uniform. This condition is fulfilled in oscillating water tunnels. However, under real waves the variation from wave crest to wave trough generates a convective acceleration of the order $\hat{u}^2/L$. The flow acceleration has order $\hat{u}/T = \hat{u}^2/L \cdot c/\hat{u}$, with $c = L/T$ the phase velocity of the wave. Since in general $c >> \hat{u}$ ($c = \sqrt{gh}$ in shallow water), $\partial u/\partial t >> u\partial u/\partial x$ and thus is the first criterion satisfied. The second criterion for horizontal uniformity in the boundary layer is that non-uniformities introduced by individual roughness elements should be restricted to a layer which is considerably thinner that the boundary layer itself (Nielsen, 1992). Since the scale of the disturbances introduced by the individual roughness elements is k_s, this may be expressed by $\delta >> k_s$. Sleath (1987) showed that over a bed of three dimensional roughness elements the ratio of the boundary layer thickness to roughness size is given approximately by:

$$\frac{\delta_{.05}}{k_s} = 0.26 \left(\frac{a}{k_s}\right)^{0.70} \tag{4.65}$$

with $\delta_{.05}$ (by definition) the top of the boundary layer ($z = \delta_{.05}$) where the velocity defect becomes less than 5% of u_∞. This expression corresponds to $\delta_{.05} = 10k_s$ for $a/k_s = 184$. Since under field conditions a is of the order 1 and $k_s \approx \eta$ of the order 0.01 this criterion seems harder to satisfy.

Another important (non-dimensional) parameter is the ratio of the orbital diameter to the ripple length: d_o/λ. If this ratio is a lot smaller than unity the vertical velocities w are small compared to the horizontal velocities u and the ripples can be simply treated as roughness elements. The vortex-ripple regime is defined by $1 \leq d_o/\lambda \leq 4$ (Malarkey & Davies, 2002). This is also confirmed by laboratory experiments; e.g. O'Donoghue & Clubb (2001) found for both sinusoidal and regular second-order Stokes waves over a large range of periods (2-10 s) and orbital velocities (0.2-0.9 ms^{-1}) that $d_o/\lambda = 1.6$-3.3. Therefore, one cannot state that it is physically justifiable to describe the hydrodynamics (and sediment dynamics) over ripples with a 1DV approach. However, from a practical point of view more sophisticated 2DV models are unduly complex and therefore 1DV models could be preferred. Recent research shows the merits of this 1DV approach (Davies & Thorne, 2002).

Chapter 5

Conclusions and recommendations

5.1 Conclusions

5.1.1 Shoreface processes

1. The sediment dynamics on the shoreface are determined by both waves (wave asymmetry) and tide- and wind-driven currents.

2. Considering the wave-related sand transport processes on the shoreface, the ripple regime is the most important (bedform) regime.

3. Wave-induced ripples on the shoreface have typical heights of 0.01-0.1 m, lengths of 0.1-1.0 m, and migration speeds of 0.01-0.1 mms^{-1}.

4. Fundamentally different processes determine sediment transport above plane and rippled beds.

5. Despite the larger onshore orbital velocities, the net wave-related transport over ripples is in most cases offshore-directed due to phase lags between velocities and concentrations caused by vortices on the lee-side of ripples.

6. The flow and sand transport above ripples can be described with the following non-dimensional quantities: d_o/D_{50}, Re_{d_o}, $\hat{u}_\mathrm{c}/\hat{u}_\mathrm{t}$, $\hat{u}_\mathrm{c}/\bar{u}$, u_*/W_f, Δ, η/λ, d_o/λ, $\theta_{2.5}$, and Φ.

5.1.2 Experiments

1. During one wave cycle two concentration peaks occur above the ripple crest and ripple trough (lower peaks, larger time lags): one just after flow reversal probably generated by lee-side vortices and one around maximum flow probably generated by stoss-side vortices.

2. The phase of eddy shedding and suspended cloud ejection is possibly linked to the orbital diameter normalized with the ripple length.

3. The velocity and concentration fields above the ripple structure are so complex, that it appears to be impossible to relate the local instantaneous sediment concentration to a local instantaneous fluid velocity.

4. There is empirical evidence that the vertical distribution of the time-averaged concentration (for symmetric, asymmetric, regular, and irregular waves) can be described with an analytical solution of the advection-diffusion equation with a constant decay length. However, proper expressions for this decay length and the reference concentration do not exist. The decay length is possibly linked to the ripple height.

5. Despite the larger onshore orbital velocities, the net wave-related transport over ripples is in most cases offshore-directed due to phase lags between velocities and concentrations caused by vortices on the lee-side of ripples.

6. The number of data sets on wave-related transport processes in the ripple regime with relatively large mobility numbers ($\Psi > 100$) and long wave periods ($T > 5$) is limited. This especially accounts for time-dependent concentration and net transport measurements.

5.1.3   Sediment transport models

1. Time-averaged and quasi-steady models are not capable to describe the wave-related sediment transport in the ripple regime.

2. Considering the present large uncertainties regarding the modeling of sediment dynamics in rippled-bed conditions, turbulence-closure models are appropriate *research* models to describe flow over ripples as a basis of sediment transport modeling.

3. Existing transport models, especially research models, are not well validated with experimental data in the ripple regime.

4. Intercomparison of both practical and research transport models shows that the greatest disagreement occurs in case of rippled beds.

5. 1DV modeling of sand transport by waves and currents in the ripple regime is a promising practical approach.

5.2   Further research

1. Performance of a new experimental series in the Large-scale Oscillating Water Tunnel at WL|Delft Hydraulics (LOWT) to obtain a data set of net transport rates and wave-related transport processes in a range of full-scale field wave conditions in the ripple regime as present on the shoreface. These experiments will be carried out with regular and irregular asymmetric oscillations over a uniform sand bed. The following parameters will be measured: ripple characteristics, net transport rates, horizontal flow velocities at various heights above the bed (above the wave boundary layer), time- and bed-averaged suspended sand concentrations, and time-dependent suspended sand concentrations at a couple of horizontal positions along the ripple.

2. Improvement of existing and development of new semi-unsteady models. The semi-unsteady models of Watanabe (1982), Nielsen (1988), and Dibajnia & Watanabe (1992); Dibajnia (1995); Dibajnia & Watanabe (1996); Silva (2001) will be compared with the new net transport data. Further model development will concentrate on wave-induced sediment dynamics in the ripple regime using the new data and other existing data sets.

3. Improvement of an existing 1DV turbulence-closure model. An existing 1DV model will be compared with the new experimental data from the LOWT experiments. Ripples are accounted for by an increased bed roughness based on the ripple dimensions and ripple effects are parameterized following the ideas of Davies & Thorne (2002). This model approach will be improved with respect to the critical issue phase of vortex shedding and sediment pick-up. The 1DV model will be validated with the new and other selected data sets.

4. Performance of a new experimental series in the Aberdeen Oscillating Flow Tunnel (AOFT) at the University of Aberdeen to investigate transport and suspension processes under both regular and irregular flow conditions. Detailed (intra-wave) measurements will be made of the velocity, ripple migration rates, and suspended sediment concentrations. This data will be used to improve and validate the semi-unsteady transport model and the 1DV model.

5. Intercomparison of the two modeling concepts. The final research activity is to assess which of the two modeling concepts (semi-unsteady, 1DV) should be preferred for practical applications. Comparisons with new and existing data sets will answer the question which model concept performs best and whether it is necessary and worthwhile to use more sophisticated, detailed, and elaborate 1DV modeling instead of semi-unsteady modeling.

Acknowledgements

Bibliography

Amos, C. L., A. J. Bowen, D. A. Huntley, & C. F. M. Lewis, Ripple generation under the combined influences of waves and currents on the canadian continental shelf, *Cont. Shelf Res.*, **8**(10):1129–1153, 1988.

Andersen, K. H., Ripples beneath surface waves and topics in shell models of turbulence, Ph.D. thesis, University of Copenhagen, Denmark, 1999.

Andersen, K. H., & J. Fredsøe, How to calculate the geometry of vortex ripples, *Coast. Sed. 1999*, 78–93, 1999.

Bagnold, R. A., Motion of waves in shallow water: interaction between waves and sand bottoms, In: *Proc. Roy. Soc. London A187*, 1–15, 1946.

Bagnold, R. A., The flow of cohesionless grains in fluids, *Phil. Trans. Roy. Soc. London*, **249**(964):235–297, 1956.

Bailard, A. A., An energetics total load transport model for a plane sloping beach, *J. Geophys. Res.*, **86**(C11):10,938–10,954, 1981.

Bijker, E. W., Longshore transport computations, *J. Waterway, Port, Coast., and Ocean Eng.*, **97**(4):687–701, 1971.

Block, M. E., A. G. Davies, & C. Villaret, Suspension of sand in oscillatory flow above ripples: discrete vortex model and laboratory experiments, In: *Sediment transport mechanisms in coastal environments and rivers Euromech 310*, 37–52, Le Havre, France, 1994.

Blondeaux, P., Mechanics of coastal forms, *Ann. Rev. Fluid Mech.*, **33**:339–370, 2001.

Blondeaux, P., E. Foti, & G. Vittori, Migrating sea ripples, *Eur. J. Mech. B-Fluids*, **19**:285–301, 2000.

Bosman, J. J., Concentration measurements under oscillatory motion, *Tech. Rep. M1695-I*, Delft Hydraulics, The Netherlands, 1981.

Bosman, J. J., Concentration measurements under oscillatory motion, *Tech. Rep. M1695-II*, Delft Hydraulics, The Netherlands, 1982.

Bosman, J. J., & H. J. Steetzel, Time- and bed-averaged concentration under waves, *Rep. 385*, Delft Hydraulics, The Netherlands, 1988.

Brørs, B., Numerical modelling of flow and scour at pipelines, *J. Hydr. Eng.*, **125**(5):511–523, 1999.

Brørs, B., & K. J. Eidsvik, Oscillatory boundary layer flows modelled with dynamic Reynolds sress turbulence closure, *Cont. Shelf Res.*, **14**(13/14):1455–1475, 1994.

Chen, Z., Sediment concentration and sediment transport due to action of waves and a current, Ph.D. thesis, Delft University of Technology, The Netherlands, 1992.

Clifton, H. E., Wave-formed sedimentary structures: a conceptual model, In: *Beach and near-shore sedimentation*, edited by R. A. Davies jr. & R. L. Ethington, 116–120, SEPM Spec. Publ. 24, 1976.

Clubb, G. S., Experimental study of vortex ripples in full-scale sinusoidal and asymmetric flows, Ph.D. thesis, Aberdeen University, UK, 2001.

Dang Huu, C., & B. T. Grasmeijer, Analysis of sand transport under regular and irregeluar waves in large-scale wave flume, *Rep. R 99-05*, University of Utrecht, The Netherlands, 1999.

Davies, A. G., & Z. Li, Modelling sediment transport beneath regular symmetrical and asymmetrical waves, *Cont. Shelf Res.*, **17**(5):555–582, 1997.

Davies, A. G., & P. D. Thorne, 1DV-model of sand transport by waves and currents in the rippled bed regime, In: *Proc. 28th Int. Conf. Coast. Eng.*, Cardiff, UK, 2002.

Davies, A. G., & C. Villaret, Oscillatory flow over rippled beds: boundary layer structure and wave-induced Eulerian drift, In: *Gravity waves in water of finite depth*, edited by J. N. Hunt, 215–254, Computational Mechanics Publications, 1997.

Davies, A. G., L. C. van Rijn, J. S. Damgaard, J. van de Graaff, & J. S. Ribberink, Intercomparison of research and practical sand transport models, *Coast. Eng.*, **46**:1–23, 2002.

Dibajnia, M., Sheet flow transport formula extended and applied to horizontal plane problems, In: *Proc. 38th Jap. Conf. Coast. Eng.*, 179–194, 1995, (in Japanese).

Dibajnia, M., & W. Watanabe, Sheet-flow under non-linear waves and currents, In: *Proc. 23rd Int. Conf. Coast. Eng.*, 2015–2025, Venice, Italy, 1992.

Dibajnia, M., & W. Watanabe, A transport rate formula for mixed sands, In: *Proc. 25th Int. Conf. Coast. Eng.*, 3791–3804, Orlando, USA, 1996.

Dibajnia, M., T. Shimizu, & W. Watanabe, Profile change of a sheet flow dominated beach, In: *Proc. 24th Int. Conf. Coast. Eng.*, 1946–1960, Kobe, Japan, 1994.

Dohmen-Janssen, C. M., Grain size influence on sediment transport in oscillatory sheet flow. Phase lags and mobile-bed effects., Ph.D. thesis, Delft University of Technology, The Netherlands, 1999.

Dohmen-Janssen, C. M., D. F. Kroekenstoel, W. N. Hassan, & J. S. Ribberink, Phase lags in oscillatory sheet flow: experiments and bed load modelling, *Coast. Eng.*, **46**:61–87, 2002.

Du Toit, C. G., & J. F. A. Sleath, Velocity measurements close to rippled beds in oscillatory flow, *J. Fluid Mech.*, **112**:71–96, 1981.

Eidsvik, K. J., Mathematical modelling of flow and suspended sediments over sand-waves using dynamic turbulence closures, In: *Sediment transport modelling in marine coastal environments*, edited by L. C. Van Rijn, A. D. Davies, J. Van de Graaff, & J. S. Ribberink, AH 1–11, Aqua Publications, Amsterdam, The Netherlands, 2001.

Engelund, F., & J. Fredsøe, A sediment transport model for straight alluvial channels, *Nordic Hydrol.*, **7**:293–306, 1976.

Everts, C. H., Geometry of profiles across inner continental shelves of the atlantic and gulf coasts of the united states, *Tech. Paper 74-4*, U.S. Army Corps of Engineers Coastal Engineering Research Center, USA, 1978.

Everts, C. H., Continental shelf evolution in response to a sea-level rise, In: *Sea-level fluctuation and coastal evolution*, edited by D. Numedal, O. H. Pilkey, & J. D. Howard, 215–254, SEPM Spec. Publ. 41, 1987.

Faraci, C., & E. Foti, Analysis of ripple evolution under regular and irregular waves trough image acquisition techniques, In: *Sediment transport modelling in coastal environments*, edited by L. C. Van Rijn, A. D. Davies, J. Van de Graaff, & J. S. Ribberink, AD 1–12, Aqua Publications, Amsterdam, The Netherlands, 2001.

Fredsøe, J., O. H. Anderson, & S. Silberg, Distribution of suspended sediment in large waves, *J. Waterway, Port, Coast., and Ocean Eng.*, **111**(6):1041–1059, 1985.

Grant, W. D., & O. S. Madsen, Movable bed roughness in unsteady oscillatory flow, *J. Geophys. Res.*, **87**(C1):469–481, 1982.

Grasmeijer, A. T., Process-based cross-shore modelling of barred beached, Ph.D. thesis, University of Utrecht, The Netherlands, 2002.

Grasmeijer, B. T., & L. C. Van Rijn, Transport of fine sand by currents and waves III: breaking waves over barred profile with ripples, *J. Waterway, Port, Coast., and Ocean Eng.*, **125**(2):71–79, 1999.

Hagatun, K., & K. J. Eidsvik, Oscillatory boundary layer with suspended sediments, *J. Geophys. Res.*, **91**(C11):13,045–13,055, 1986.

Hansen, E. A., J. Fredsøe, & R. Deigaard, Distribution of suspended sediment over wave-generated ripples, *J. Waterway, Port, Coast., and Ocean Eng.*, **120**:37–55, 1994.

Hassan, W. N., Transport of size-graded and uniform sediments under oscillatory sheet-flow conditions, Ph.D. thesis, University of Twente, The Netherlands, 2003.

Hassan, W. N., D. F. Kroekenstoel, J. S. Ribberink, & L. C. Van Rijn, Gradation effects on sand transport under oscillatory sheet-flow conditions, *Data report Series P*, University of Twente, The Netherlands, 1999.

Holmedal, L. E., Wave-current interactions in the vicinity of the sea bed, Ph.D. thesis, NTNU Trondheim, Norway, 2002.

Huyn Thanh, S., & A. Temperville, A numerical model of the rough turbulent boundary layer in combined wave and current interaction, In: *Proc. 22rd Int. Conf. Coast. Eng.*, 853–866, Delft, The Netherlands, 1990.

Huyn Thanh, S., T. Tran Thu, & A. Temperville, A numerical model for suspended sediment in combined currents and waves, In: *Sediment transport mechanisms in coastal environments and rivers Euromech 310*, 37–52, Le Havre, France, 1994.

Janssen, C. M., Sand transport in oscillatory sheet-flow. A literature review., *Communications on hydraulic and geotechnical engineering*, Delft University of Technology, The Netherlands, 1995.

Jensen, B. L., B. M. Summer, & J. Fredsøe, Turbulent oscillatory boundary layers at high Reynolds numbers, *J. Fluid Mech.*, **206**:265–297, 1989.

Jonsson, I. G., Wave boundary layers and friction factors, In: *Proc. 10th Int. Conf. Coast. Eng.*, 127–148, Tokyo, Japan, 1966.

Jonsson, I. G., A new approach to oscillatory rough turbulent boundary layers, *Ocean Eng.*, **7**:109–152, 1980.

Kajiura, K., A model of the bottom boundary layer in water waves, *Bull. Earthquake Res. Inst.*, **46**:75–123, 1968.

Katopodi, I., J. S. Ribberink, P. Ruol, H. Koelwijn, C. Lodahl, S. Longo, A. Crosato, & H. Wallace, Intra-wave sediment transport in an oscillatory flow superimposed on a mean current, *Tech. Rep. H1684-III*, Delft Hydraulics, The Netherlands, 1994.

Kleinhans, M. G., Sediment dynamics on the shoreface and upper continental shelf. A review., *Tech. rep.*, Physical Geography, University of Utrecht, The Netherlands, 2002.

Koelewijn, H., Sediment transport under sheet-flow conditions, M.Sc. thesis, Delft University of Technology, The Netherlands, 1994.

Kroon, A., Sediment transport and morphodynamics of the beach and nearshore zone near Egmond, The Netherlands, Ph.D. thesis, University of Utrecht, The Netherlands, 1994.

Li, Z., & A. G. Davies, Towards predicting sediment transport in combined wave-current flow, *J. Waterway, Port, Coast., and Ocean Eng.*, **124**(4):157–164, 1996.

Longuet-Higgins, M. S., Oscillatory flow over steep sand ripples, *J. Fluid Mech.*, **107**:1–35, 1981.

Madsen, O. S., & W. D. Grant, Sediment transport in the coastal environment, *Rep. 209*, Massachusetts Inst. of Tech., UK, 1976.

Madsen, O. S., L. D. Wright, J. S. Boon, & T. A. Chisholm, Wind stress, bed roughness, and sediment suspension on the inner shelf during an extreme storm event, *Cont. Shelf Res.*, **13**(11):1303–1324, 1993.

Malarkey, J., Modelling oscillatory flow over vortex ripples using the discrete vortex method, Ph.D. thesis, University of Wales, UK, 2001.

Malarkey, J., & A. G. Davies, Discrete vortex modelling of oscillatroy flow over ripples, **24**:127–145, 2002.

McFetridge, W. F., & P. Nielsen, Sediment suspension by non-breaking waves over rippled beds, *Tech. Report UFL/COEL-85/005*, University of Florida, USA, 1985.

Meyer-Peter, E., & R. Müller, Formulas for bed-load transport, In: *Report of 2nd Meeting of the International Association of Hydraulic and Structural Research*, 39–64, Stockholm, Sweden, 1948.

Mogridge, G. R., & J. W. Kamphuis, Experiments on bed form generation by wave action, In: *Proc. 13th Int. Conf. Coast. Eng.*, 1123–1142, Vancouver, Canada, 1972.

Mogridge, G. R., M. H. Davies, & D. H. Willis, Geometry prediction for wave-generated bedforms, *Coast. Eng.*, **22**:225–286, 1994.

Niedoroda, A. W., & D. J. P. Swift, Shoreface processes, In: *Handbook of coastal and ocean engineering, Vol. 2*, edited by J. B. Herbich, 735–770, Gulf Publishing Company, Houston, USA, 1991.

Nielsen, P., Some basic concepts of wave sediment transport, *Series paper no. 20*, Techical University of Denamrk, Denmark, 1979.

Nielsen, P., Dynamics and geometry of wave-generated ripples, *J. Geophys. Res.*, **86**(C7):6467–6472, 1981.

Nielsen, P., Field measurements of time-averaged suspended sediment concentrations under waves, *Coast. Eng.*, **8**:51–72, 1984.

Nielsen, P., Suspended sediment concentrations under waves, *Coast. Eng.*, **10**:23–31, 1986.

Nielsen, P., Three simple models of wave sediment transport, *Coast. Eng.*, **12**:43–62, 1988.

Nielsen, P., Coastal bottom boundary layers and sediment transport, In: *Port Engineering*, edited by P. Bruun, fourth ed., 550–585, 1990.

Nielsen, P., *Coastal bottom boundary layers and sediment transport*, World Scientific, Singapore, 1992.

O'Donoghue, T., & G. S. Clubb, Sand ripples by regular oscillatory flow, *Coast. Eng.*, **44**:101–115, 2001.

Perrier, G., Numerical modelling of the flow and sand transport by waves and currents over a rippled bed, Ph.D. thesis, Orsay Université, France, 1996.

Ramadan, K. A. H., Time-averaged sediment transport phenomena in combined wave-current flow, *Tech. Rep. H1889-I*, Delft Hydraulics, The Netherlands, 1994.

Raudkivi, A. J., *Loose boundary hydraulics*, third ed., Pergamon, Oxford, UK, 1990.

Ribberink, J. S., Influence of wave-asymmetry and wave-irregularity of time- and bed-averaged sediment concentrations, *Note H186.00-1*, Delft Hydraulics, The Netherlands, 1987.

Ribberink, J. S., Sediment transport induced by the near-bed wave orbital motion, theory and experiments. A literature review., *Tech. Rep. H840*, Delft Hydraulics, The Netherlands, 1989.

Ribberink, J. S., Time-averaged sediment transport phenomena in combined wave-current flow, *Tech. Rep. H1889-II*, Delft Hydraulics, The Netherlands, 1995.

Ribberink, J. S., Bed-load transport for steady flows and unsteady oscillatory flows, *Coast. Eng.*, **34**:59–82, 1998.

Ribberink, J. S., & A. A. Al-Salem, Bedform, near-bed sediment concentration and sediment transport in simulated regular wave conditions, *Tech. Rep. H840-III*, Delft Hydraulics, The Netherlands, 1989.

Ribberink, J. S., & A. A. Al-Salem, *Near-bed sediment transport and suspended concentration under waves*, Int. Symp. on: 'The transport of suspended sediments and its mathematical modelling', Florence, Italy, 1991a.

Ribberink, J. S., & A. A. Al-Salem, Sediment transport, sediment concentrations and bedforms in simulated asymmetric wave conditions, *Tech. Rep. H840-IV*, Delft Hydraulics, The Netherlands, 1991b.

Ribberink, J. S., & A. A. Al-Salem, Sediment transport, sediment concentrations and bedforms in simulated asymmetric wave motion, *Tech. Rep. H840-V*, Delft Hydraulics, The Netherlands, 1992.

Ribberink, J. S., & A. A. Al-Salem, Sediment transport in oscillatory boundary layers in case of rippled beds and sheet flow, *J. Geophys. Res.*, **99**(C6):12,707–12,727, 1994.

Ribberink, J. S., & Z. Chen, Sediment transport of fine sand under asymmetric oscillatory flow. Part VII., *Tech. Rep. H840-VII*, Delft Hydraulics, The Netherlands, 1993.

Richardson, Y. F., & W. N. Zaki, Sedimentation and fluidization, *Trans. Inst. Chem. Eng.*, **32**(1):35–53, 1954.

Sandpit project partners, Sand transport and morphology of offshore sand mining pits/areas, *Technical Annex*, 2001.

Sato, S., Oscillatory boundary layer flow and sand movement over ripples, Ph.D. thesis, University of Tokyo, Japan, 1987.

Sato, S., N. Mimura, & A. Watanabe, Oscillatory boundary layer flow over a rippled bed, In: *Proc. 19th Int. Conf. Coast. Eng.*, 2293–2309, Houston, USA, 1984.

Sawamoto, M., & T. Yamashita, Sediment transport due to wave action, *J. Hydrosc. Hydraul. Eng.*, **14**(1):1–15, 1986.

Scandura, P., G. Vittori, & P. Blondeaux, Three dimensional flow over steep ripples, *J. Fluid Mech.*, **412**:285–378, 2000.

Schepers, J. D., Zandtransport onder invloed van golven en een eenparige stroom bij varierende korreldiameter, M.Sc. thesis, Delft University of Technology, The Netherlands, 1978, (in Dutch).

Schlichting, H., *Boundary layer theory*, seventh ed., McGraw-Hill, New York, USA, 1979.

Sheng, Y. P., Hydraulic applications of a second-order closure model of turbulent transport, In: *Conf. Applying Res. to hydr. Practice*, Jackson, USA, 1982.

Silva, P. A., Contributions to the study of sedimentation in coastal regions, Ph.D. thesis, University of Aveiro, Portugal, 2001, (in Portuguese).

Silva, P. A., P. A. Mendes, J. Antunes do Carmo, & F. Seabra Santos, Medições de campos velocidades num escoamento oscilató rio sobre um fundo com rugas, *Tech. Rep. IV*, Silusba, Coimbra, 1999.

Sistermans, P. G. J., Graded sediment transport by waves and a current, Ph.D. thesis, Delft University of Technology, The Netherlands, 2002.

Sleath, J. F. A., Turbulent oscillatory flow over rough beds, *J. Fluid Mech.*, **182**:369–409, 1987.

Sleath, J. F. A., Ripple geometry under severe wave conditions, In: *Proc. 27th Int. Conf. Coast. Eng.*, 2686–2699, Sydney, Australia, 2000.

Soulsby, R., *Dynamics of marine sands*, Telford, London, UK, 1997.

Steetzel, H. J., Sedimentsuspensie in een oscillerende waterbeweging vlak boven het zandbed, M.Sc. thesis, Delft University of Technology, The Netherlands, 1984, (in Dutch).

Sunamura, T., Laboratory study of on-offshore transport rate in shallow water region, In: *Proc. 29th Jap. Conf. Coast. Eng.*, 239–243, 1982, (in Japanese).

Suzuki, K., A. Watanabe, M. Isobe, & M. Dibajnia, Experimental study on transport of sediment with mixed-grain size due to oscillatory flow, In: *Proc. 41st Jap. Conf. Coast. Eng.*, 356–360, 1994, (in Japanese).

Swart, D. H., Offshore sediment transport and equilibrium beach profiles, *Delft Hydr. Lab. Publ. 131*, Delft Hydraulics, The Netherlands, 1974.

Thorne, P. D., J. J. Williams, & A. G. Davies, Suspended sediment under waves measured in a large-scale flume facility, *J. Geophys. Res.*, **107**(C8), 2002.

Tilmans, W., Zandtransport in de golfrichting in relatief ondiep water, M.Sc. thesis, Delft University of Technology, The Netherlands, 1979, (in Dutch).

Uittenbogaard, R. E., J. Bosboom, & T. Van Kessel, Numerical simulation of wave-current driven sand transport, revised edition, *Rep. Z2899.10*, Wl|Delft Hydraulics, The Netherlands, 2000.

Utnes, T., & T. S. Meling, Treatment of turbulent wall boundary conditions using linear-logarithmic elements, *Comp. Meth. Appl. Mech. Eng.*, **169**:123–134, 1999.

Van der Werf, J. J., Sand transport under shoreface conditions. Explorative analyses., *Tech. rep.*, University of Twente, The Netherlands, 2002, (unpublished).

Van Rijn, L. C., *Principles of sediment transport in rivers, estuaries, and coastal seas*, Aqua Publications, Amsterdam, The Netherlands, 1993.

Van Rijn, L. C., A. D. Davies, J. Van de Graaff, & J. S. Ribberink, *Sediment transport modelling in coastal environments*, Aqua Publications, Amsterdam, The Netherlands, 2001.

Vittori, G., & V. Armenio, Large eddy simulation of oscillatory boundary layers, In: *Proc. 4th Euromech Fluid Mech. Conf.*, Eindhoven, The Netherlands, 2000.

Vongvisessomjai, S., Oscillatory ripple geometry, *J. Hydr. Eng.*, **110**(3):246–266, 1984.

Watanabe, A., Numerical models of nearshore currents and beach deformation, **25**:147–161, 1982.

Watanabe, A., & M. Isobe, Sand transport rate under wave-current action, In: *Proc. 22nd Int. Conf. Coast. Eng.*, 2495–2507, Delft, The Netherlands, 1990.

Whitehouse, R. J. S., M. F. C. Thorn, & P. J. Houghton, Sediment transport measurements at Maplin Sands, Outer Thames Estuary, *Rep. TR 15*, HR Wallingford, UK, 1996.

Whitehouse, R. J. S., M. W. Owen, & E. C. Stevenson, Sediment transport measurements at Boscombe Pier, Poole Bay, *Rep. TR 27*, HR Wallingford, UK, 1997.

Wiberg, P. L., & C. K. Harris, Ripple geometry in wave-dominated environments, *J. Geophys. Res.*, **99**(C1):775–789, 1994.

Williams, J. J., C. P. Rose, P. D. Thorne, L. E. Coates, J. R. West, P. J. Hardcastle, , J. D. Humphrey, S. P. Moores, & D. J. Wilson, Observed suspended sediments in storm conditions, In: *Proc. 25th Int. Conf. Coast. Eng.*, 3527–3269, Orlando, USA, 1997.

Wolf, F. C. J., Hydrodynamics, sediment transport and daily morphological development of a bar-beach system, Egmond, The Netherlands, Ph.D. thesis, University of Utrecht, The Netherlands, 1997.

Zyserman, J. A., & J. Fredsøe, Data analysis of bed concentration of suspended sediment, *J. Hydr. Eng.*, **120**(9):1021–1042, 1994.

List of symbols

Roman symbols

a	semi-excursion length of orbital motion
c_0	near-bed reference concentration
$c(x, z, t)$	time-dependent suspended sediment concentration
$c(z)$	time- and bed-averaged suspended sediment concentration
$c(z, t)$	time-averaged suspended sediment concentration
D_*	non-dimensional grain size
D_{50}	median grain size
d_o	orbital diameter
f	friction factor
g	acceleration due to gravity
h	water depth
H	wave height
k	wave number
k_s	Nikuradse roughness height
q_s	sediment transport rate
p	pressure
P	phase lag parameter
r_c	concentration decay length
R	rate of asymmetry
Re	Reynolds number
T	wave period
T_c	wave crest period
T_p	peak period of wave spectrum
T_t	wave trough period
u	velocity in x-direction
u_*	friction velocity
$\hat{u}_1$	orbital velocity amplitude of first harmonic
$\hat{u}_2$	orbital velocity amplitude of second harmonic
u_c	equivalent sinusoidal velocity under wave crest
$\hat{u}_\mathrm{c}$	orbital velocity amplitude under wave crest
$\bar{u}_\mathrm{s}$	Stokes velocity
$\hat{u}_\mathrm{t}$	orbital velocity amplitude under wave trough
v	velocity in y-direction
w	velocity in z-direction
W_f	sediment particle fall velocity
x	horizontal coordinate in wave direction
y	horizontal coordinate perpendicular to the x-direction
z	vertical coordinate
z_b	near-bed reference level
z_0	zero-intercept level of logarithmic velocity profile

Greek symbols

δ	boundary layer thickness
δ_s	Stokes length
δ_{sf}	sheet-flow layer thickness
Δ	relative density of sediment
ε_m	molecular sediment diffusivity
ε_t	turbulent sediment diffusivity
η	ripple height
θ	Shields parameter
κ	Von Karman constant
λ	ripple length
ν_m	molecular viscosity
ν_t	turbulent eddy viscosity
ρ	density of water
ρ_s	density of sediment
σ_g	geometric standard devistion
τ_b	bed shear stress
Φ	non-dimensional transport parameter
χ	wave period parameter
Ψ	mobility number
ω	angular frequency

General operators

$^-$	time-averaged, steady component
$^\sim$	periodic component
$'$	random component
$^\wedge$	peak value

Subscripts

c	pertaining to currents
cr	critical value
max	maximum value
min	minimum value
rms	root mean square value
s	pertaining to sediment
w	pertaining to waves